이차원 할로겐화물 페로브스카이트 기반 상용 수준 고효율 고안정성 광변환 소자 제작

Highly efficient and stable solar cells based on two-dimensional perovskite

2023년 2월

서울대학교 대학원

기계항공공학부

장 연 우

이차원 할로겐화물 페로브스카이트 기반 상용 수준 고효율 고안정성 광변환 소자 제작

Highly efficient and stable solar cells based on two-dimensional perovskite

지도교수 최만수

이 논문을 공학박사 학위논문으로 제출함

2022년 10월

서울대학교 대학원

기계항공공학부

장 연 우

장연우의 공학박사 학위논문을 인준함

2022년 12월

위 원 장 :   이 윤 석   (인)

부위원장 :   최 만 수   (인)

위   원 :   박 상 욱   (인)

위   원 :   강 성 민   (인)

위   원 :   우 창 규   (인)

Highly efficient and stable solar cells based on two-dimensional perovskite

Yeoun-Woo JANG

Department of Mechanical Engineering

The Graduate School

Seoul National University

Abstract

In order for the perovskite solar cell to emerge as a next-generation solar cell, it is necessary to research a technology that can realize large-area while obtaining efficiency and stability at the same time. At this time, it is very interesting that a material with a different dimension can be obtained as a result of only changing the crystal arrangement without destroying the halide structure by changing the organic cation of perovskite to a slightly larger spacer. Although the diversity of the two-dimensional (2D) perovskite produced in this way is infinite depending on the type of spacer, most of the 2D perovskite has a more organic surface state than the three-dimensional (3D) perovskite. This special surface blocks the external environment and the inner layer, giving the photoactive layer resistance to the external environment. Because of these properties, 2D perovskite has attracted the attention of many researchers who have tried to solve the stability problem that solar cells have suffered from, and numerous studies have been conducted on how to properly use the

material. In the process, it is found that the 2D perovskite alone has a conflicting effect of stability and efficiency, but only the advantages of each material can be obtained by well-coordinating the bonding between the 3D perovskite and the 2D perovskite. The structure is called a 2D perovskite : 3D perovskite junction structure, and with the additional surface defect control effect provided by the structure, a solar cell with a commercial level of efficiency of 20% or more was produced with only perovskite material. However, processes based on an inexperienced level of understanding of 2D perovskite were still insufficient to obtain the operating stability of the device

Therefore, I devised a Solid state In-plane Growth method (SIG process) using a solid-state precursor based on the classical crystal formation theory, and through this, I succeeded in making a whole 2D perovskite : 3D perovskite structure. In the process of making the structure, interface damage was not only removed, but also the depletion layer was optimized using the property of a hole-dominant material, and an optimized device structure was presented through the same material. The device has recorded the highest efficiency as an international certification among solar cell devices using a 2D perovskite : 3D perovskite junction structure so far, and also showed the world's highest level of stability. The technology can be further developed in stages when the properties of two-dimensional perovskite are understood and the growth principle is quantified, and it can be applied to various devices.

Solar cell devices already show driving performance beyond efficiency based on the Shockley-Queisser theory. This is because the light emitting mechanism inside the device absorbs and emits light in several stages, such as light recycling and scattering. Recognizing this fact, we should

understand solar cells from the perspective of a good luminous body, which requires more effort to raise the value of how well electrons are emitted as light, called ELQE (Electroluminescence Quantum Efficiency). To this end, I studied light recycling and scattering in devices beyond the Shockley-Queisser threshold and methods for measuring charge diffusivity in two-dimensional perovskites and 3D perovskites. The SIG process is also a method that can control the amount of emission light that is lost in dispersion in the device through thickness control. In addition, research on an anti-reflection film capable of increasing the amount of light incident into the device was also conducted. With the information obtained by continuing research on the synthesis or physical properties of 2D perovskite, I will continue to try to utilize the structure of 2D perovskite: 3D perovskite to a level that can be used for large-area commercial devices. In order to realize a commercially available device while maintaining high stability and high efficiency, the device structure must be designed under the concept that the perovskite is a good light emitting material, and research on the physical properties of 2D perovskite must be preceded.

Table of Contents

List of Tables

List of Figures

Nomenclature

2D : 2-dimensional

3D : 3-dimensional

n : N number

PR : photon recycling

ELQE : Electroluminescence Quantum Efficiency

RH: Relative humidity $\hspace{6cm}$ [%]

VOC : open circuit voltage $\hspace{5.5cm}$ [V]

JSC: Short circuit current $\hspace{4.5cm}$ [mA cm^{-2}]

FF : fill factor $\hspace{7cm}$ [%]

PCE : power conversion efficiency $\hspace{4cm}$ [%]

PR : photon recycling

Chapter 1. Introduction

1.1. Background

1.1.1. Perovskite Solar Cell (PSC)

The perovskite mineral was discovered in the Ural Mountains of Russia by Gustav Rose in 1839 and named after the Russian mineralogist Lev Perovski (1792-1856). The crystal structure of perovskite was first described in 1926 in Victor Goldschmidt's study of the tolerance factor, and its crystal structure was revealed in the X-ray diffraction study of barium titanate by Helen Dick Megaw [1]. Common perovskite refers to 3D (3-Dimensional) perovskite and has a crystal structure of the same type as ABX3. [2] Among them, a structure in which small ammonium chains at the A site, a metal such as Pb^{2+} or Sn^{2+} at the B site, and a halide at the X site are called metal halide perovskite, (Figure 1) It has received great attention because of its good light conversion properties.

The development of perovskite material-based solar cells began in 2009 by Tsutomu Miyasaka's research team using a halogen perovskite material as a photoactive layer, showing an efficiency of

1

3.81%. The use of lead-containing halogen perovskite rather than fuel-sensitized solar cells using a porous TiO2 film made it possible to have high photoelectric conversion efficiency much more easily than conventional organic solar cells. [3]. After that, in 2012, Michael Grätzel and Park Nam-gyu's team reported 9% photoelectric conversion efficiency and started research on high-efficiency solar cells [4]. As a result of various studies being actively conducted, an efficiency of up to 25.7% is currently reported [5].

The biggest advantage when using the perovskite structure as a photoactive part is that it has an open circuit voltage of 1.0V to 1.2V, which is much higher than the open circuit voltage of 0.6V to 0.7V of the existing organic solar cells, and the light absorption is also very high. In addition, the theoretical photoelectric conversion efficiency is greatly increased and the thin film fabrication method is very simple, making it easy to fabricate solar cell devices [6]. It is attracting attention as a next-generation solar cell, and is currently in the stage of taking the first step to commercialization by maintaining high efficiency and succeeding in stability and large area at the same time.
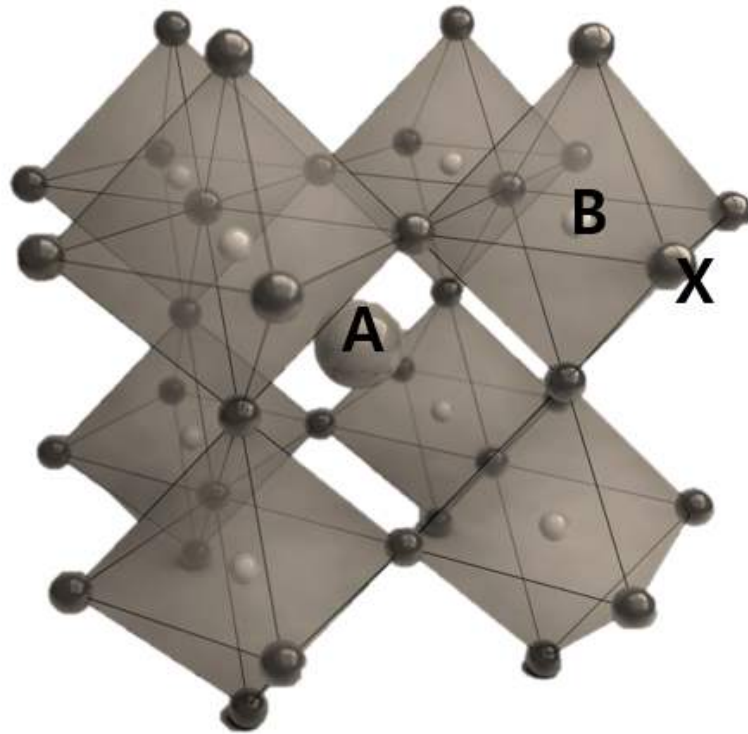
Figure 1. The structure of Metal halide perovskite

1.1.2. 2D perovskite

The 2D (2-Dimensional) perovskite, fabricated by chemical dimensional reduction of the 3D perovskite lattice, forms a new dimensional structure of $(A')_m(A)_{n-1}B_nX_{3n+1}$. A is a large organic cation, A is a small cation such as methylammonium (MA) or formamidinium (FA), B is a metal such as Pb^{2+} and Sn^{2+}, and X is a halide material. (Figure 2) Here, the monovalent (m = 2) or divalent (m = 1) cation can be inserted between the octahedral structure layer sheets made by B and Halide. A variation of halide with a wide variety of organic components essentially allows easy access to hybrid organic-inorganic materials as well as fine-tuning of their optoelectronic properties. [7] In 2D halide perovskites, organic cations act as insulating barriers that limit the movement of charge carriers into dimensions and form 2D multi-quantum wells. It also acts as a dielectric regulator to determine the electrostatic forces applied to photogenic electron-hole pairs. The massive electron-hole binding energy formed by the high organic/inorganic dielectric constant contrast originally present in 3D perovskite is further enhanced in 2D perovskite. A characteristic property of 2D perovskite is the trade-off between surface energy and carrier conductivity, dependent on N numbers. (meaning the degree of

4

repetition of the metal halide octahedral structure layer and the organic layer) [8] In fact, as the number of N decreases, the chemical properties change stably, but the carrier movement becomes increasingly difficult.

Depending on the type of organic cation, the way the octahedral layer is woven changes, and the (100) oriented perovskite structure is common. In particular, the main focus of research is on the interstructural correlation of 2d perovskite along the crystal structure of Ruddlesden-Poper (RP), [9, 10] Dion-Jacobson (DJ), [11] and alternating interlayer space (ACI) [12]. Currently, 2D Perovskite is widely used in light emitting diodes (LEDs), (13, 14) and photodetectors. [15, 16] 2D nanocrystals [17,18] and has made a big mark in high-efficiency, high-stability photoboltic production [19, 20] using chemistry with 3D perovskite.
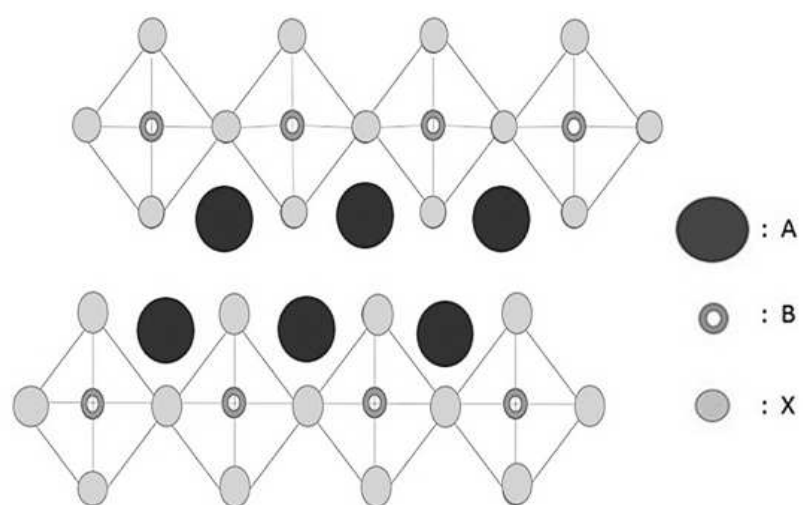
Figure 2. Structure of 2D perovsktie (Ruddlesden-popper structure)

1.1.3. 2D:3D structure

The above-mentioned 2D perovskite has a superior stability than 3D perovskite and has attracted strong interest in commercializing devices. However, unlike the exciton binding energy of 3D perovskite, which is only 10 meV, that of 2D perovskite is almost 500 meV, which is several orders of magnitude higher. This means that adopting 2d perovskite inevitably causes a trade-off between efficiency and stability. Therefore, in order to solve this problem, the following four methods were adopted as a method of using 2D as an optical active unit. 1) Improving the properties of 2D perovskite, 2) Using Quasi-2D perovskite 3) Applying 2D to the passivation area around 3D grain 4) Using 2D:3D structure. Among them, the 2D:3D structure is adopted because the structure can only increase the stability while maintaining the light conversion properties of the 3D perovskite. In particular, in the case of the 2D:3D structure, the problem of reducing the carrier life time due to non-radiative recombination was somewhat solved, and even an increase in efficiency was observed. It can be said that it is a method of simultaneously obtaining stability and efficiency, which are two important tasks for commercialization. If we can create a full 2D:3D junction, we can analyze the mechanism of the interface. The electric field distribution, the most important consideration in photovoltaic manufacturing, is determined by

semiconductor properties such as carrier concentration and work function of two- and three-dimensional perovskite layers. Many studies report bandgap configurations and working functions for 2D and 3D perovskite through UV absorption spectra and energy band analysis. [5,6] In particular, the $FAPbI_3$-based perovskite used in my experiments was reported to be a p-type material. [7,8] Actually measured UV photoelectron spectroscopy results also show that the Fermi level (4.81 eV) is slightly below the midpoint between the conduction band minimum (CBM) of 4.01 eV and the valence band maximum (VBM) of 5.56 eV. (Figure 3) In the case of 2d perov, it was also revealed that it is a p-type material. [9]

Therefore, 2D:3D junctions are considered p-p isotype heterojunctions. According to the Anderson model, these heterojunctions are classified into different types according to their bandgap position and work function electron affinity. The case I'm dealing with is the case where the bandgap of 2D perovskite is larger than that of 3D perovskite and the work function is much deeper. Here, the junction is the intrinsic hole movement from the field induction layer to the light absorption layer when the p-p heterojunction is formed, and this movement is related to the built-in potential (Vbi) of the depletion region. For p-p heterojunctions composed of 2D:3D, Vbi increases with thickness until the broadband

gap p-type layer is completely depleted. In addition, Vbi is related to the difference between the different carrier concentrations in the 2D layer and the carrier concentration in the 3D layer, and varies more with the thickness of the 2D layer, which has a relatively low intrinsic carrier concentration. That is, there is a 2D thickness to form a sufficient depletion, which means that a 2D:3D bilayer fabrication method that can control the thickness is required.
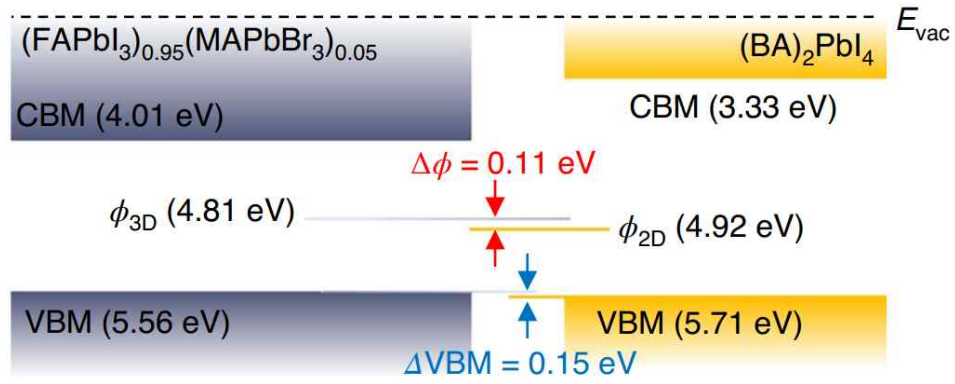
Figure 3. Energy level band alignment between the 3D perovskite and (BA)2PbI4.

1.1.4. Commercialization issue

In commercializing high-efficiency devices, it is important to find the golden triangle of three factors that match efficiency, stability, and reasonable process cost.[21] The potential of perovskite solar cell (PSC) as high-efficiency devices is evident from the rapid increase in PCE from 3.8% to 25.7% within 10 years. The path to efficiency improvement has been through modification of the device architecture, material determination of ETL and HTL, and the absorber layer. [22-24] Since efficiency and stability are largely dependent on thin film fabrication technology, it is important to develop various manufacturing technologies. Research on scale-up technology and modulation that can apply the technology to large area devices is also important.

Improving the quality of the perovskite film is the most decisive factor in determining the performance of PSC, and various methods including additive and lewis base methods have been studied. In fact, X-ray diffraction studies have revealed that the activation energy of perovskite ($56.6 \sim 97.3$ kJmol^{-1}) is very low, enabling various low temperature processes. [25] However, the technology studied so far basically uses spin coating, but this technology cannot be used to manufacture large area devices. Processes for large-area expansion

and modulation should be also studied.

In addition to the high efficiency and low cost commercialization process, the stability of the device is the important thing. Factors that affect device stability include oxygen, moisture, temperature, lighting, bias, and UV. [26] Moisture induced instability is usually caused by the hygroscopic properties of amine salts, so that the perovskite in contact with moisture decomposes into the original ammnium halide and metal halides such as PbI2, and ultimately forms the volatile amine.[27] Moisture and oxygen contact of PSCs can simply be avoided by using encapsulation of PSCs. [28] However, encapsulation increases the overall cost of the device and cannot protect the device from the harmful effects imposed by other factors such as light, heat, lighting and bias. [29]

The operating temperature range of solar cells is 40 °C to 85 °C, so solar cells must have the ability to withstand high temperature conditions. $MAPbI_3$ has low thermal conductivity and decomposes at a temperature of 85 °C even in an inert atmosphere. [30] Since all solar cells have to go through lighting and electrical bias in order to produce electricity, degradation due to lighting may occur. In particular, TiO_2, which is widely used as ETL, can be a potential photocatalyst due to its redox properties. Other factors including layer additives, charge selective interfaces and electrical biasing can

1 2

be a another threat. [31] The toxicity of Pb metal used in most devices is also a problem, and methods to solve this problem are also attracting attention. [32, 33]

1.2. Research objectives

This dissertaion aims to understand the role of 2d perovskite as a cornerstone for successful commercialization of high-efficiency solar cells, devise the best way to use them, and confirm the results. In Chapter 2, we will discuss the concepts and values of the SIG(Solid state Inplane Growth) process. It will be understood that the SIG process is the most scientific way to form a 2D:3D perovskite structure and is a complete technology that exceeds all the limitations of the existing technology. Observe the properties of the 2d:3d structures formed by the technology and understand the future potential obtained by improving and developing the process.

In Chapter 3, we will talk about the key factor needed to create a more efficient device in the future. I will introduce my existing research approach centered on ELQE. In addition, future research directions are presented and the corresponding analysis tools are also included. Through this, it is possible to understand the exact direction to create high-efficiency devices and devise an appropriate fabrication process.

In Chapter 4, we will discuss how to effectively solve many of the problems of commercialization presented above. The experimental process centered on stability and large-area modularization will be

introduced, and commercial devices at the current level will be presented.

In Chapter 5, I will summarize the contents mentioned in this dissertaion and discuss the value of the studies conducted and future research directions.

1.3. References

[1] Goldschmidt, V. M. (1926). Die gesetze der krystallochemie. Naturwissenschaften, 14(21), 477-485.

[2] Wenk, H. R., & Bulakh, A. (2016). Minerals: their constitution and origin. Cambridge University Press.

[3] Kojima, A., Teshima, K., Shirai, Y., & Miyasaka, T. (2009). Organometal halide perovskites as visible-light sensitizers for photovoltaic cells. Journal of the american chemical society, 131(17), 6050-6051.

[4] Kim, H. S., Lee, C. R., Im, J. H., Lee, K. B., Moehl, T., Marchioro, A., ... & Park, N. G. (2012). Lead iodide perovskite sensitized all-solid-state submicron thin film mesoscopic solar cell with efficiency exceeding 9%. Scientific reports, 2(1), 1-7.

[5] Best Research-Cell Efficiencies (NREL, 2022); https://www.nhttps://www.nrel.gov/pv/assets/pdfs/best-research-cell-efficiencies-rev220630.pdf

[6] Elumalai, N. K., Mahmud, M. A., Wang, D., & Uddin, A. (2016). Perovskite solar cells: progress and advancements. Energies, 9(11), 861.

[7] Aleksandrov, K. S. (1995). Structural phase transitions in layered perovskitelike crystals. Crystallography Reports, 40(2).

[8] Quan, L. N., Yuan, M., Comin, R., Voznyy, O., Beauregard, E. M., Hoogland, S., ... & Sargent, E. H. (2016). Ligand-stabilized reduced-dimensionality perovskites. Journal of the American Chemical Society, 138(8), 2649-2655.

[9] Stoumpos, C. C., Cao, D. H., Clark, D. J., Young, J., Rondinelli, J. M., Jang, J. I., ... & Kanatzidis, M. G. (2016). Ruddlesden-Popper hybrid lead iodide perovskite 2D homologous semiconductors. Chemistry of Materials, 28(8), 2852-2867.

[10] Stoumpos, C. C., Soe, C. M. M., Tsai, H., Nie, W., Blancon, J. C., Cao, D. H., ... & Kanatzidis, M. G. (2017). High members of the 2D Ruddlesden-Popper halide perovskites: synthesis, optical properties, and solar cells of (CH3 (CH2) 3NH3) 2 (CH3NH3) 4Pb5I16. Chem, 2(3), 427-440.

[11] Mao, Lingling, Weijun Ke, Laurent Pedesseau, Yilei Wu, Claudine Katan, Jacky Even, Michael R. Wasielewski, Constantinos C. Stoumpos, and Mercouri G. Kanatzidis. "Hybrid Dion-Jacobson 2D lead iodide perovskites." Journal of the American Chemical Society 140, no. 10 (2018): 3775-3783.

[12] Soe, Chan Myae Myae, Constantinos C. Stoumpos, Mikaël Kepenekian, Boubacar Traoré, Hsinhan Tsai, Wanyi Nie, Binghao Wang et al. "New type of 2D perovskites with alternating cations in the interlayer space,(C (NH2) 3)(CH3NH3) n Pb n I3 n+ 1: Structure,

properties, and photovoltaic performance." Journal of the American Chemical Society 139, no. 45 (2017): 16297-16309.

[13] Wang, N., Cheng, L., Ge, R., Zhang, S., Miao, Y., Zou, W., ... & Huang, W. (2016). Perovskite light-emitting diodes based on solution-processed self-organized multiple quantum wells. Nature Photonics, 10(11), 699-704.

[14] Quan, L. N., Zhao, Y., García de Arquer, F. P., Sabatini, R., Walters, G., Voznyy, O., ... & Sargent, E. H. (2017). Tailoring the energy landscape in quasi-2D halide perovskites enables efficient green-light emission. Nano letters, 17(6), 3701-3709.

[15] Sun, C., Xu, G., Jiang, X. M., Wang, G. E., Guo, P. Y., Wang, M. S., & Guo, G. C. (2018). Design strategy for improving optical and electrical properties and stability of lead-halide semiconductors. Journal of the American Chemical Society, 140(8), 2805-2811..

[16] Han, S., Wang, P., Zhang, J., Liu, X., Sun, Z., Huang, X., ... & Luo, J. (2018). Exploring a polar two-dimensional multi-layered hybrid perovskite of (C5H11NH3) 2 (CH3NH3) Pb2I7 for ultrafast-responding photodetection. Laser & Photonics Reviews, 12(8), 1800060.

[17] Weidman, M. C., Goodman, A. J., & Tisdale, W. A. (2017). Colloidal halide perovskite nanoplatelets: an exciting new class of semiconductor nanomaterials. Chemistry of Materials, 29(12),

5019−5030.

[18] Dou, L., Wong, A. B., Yu, Y., Lai, M., Kornienko, N., Eaton, S. W., ... & Yang, P. (2015). Atomically thin two−dimensional organic−inorganic hybrid perovskites. Science, 349(6255), 1518−1521.

[19] Smith, I. C., Hoke, E. T., Solis-Ibarra, D., McGehee, M. D., & Karunadasa, H. I. (2014). A layered hybrid perovskite solar-cell absorber with enhanced moisture stability. Angewandte Chemie International Edition, 53(42), 11232−11235.

[20] Jang, Y. W., Lee, S., Yeom, K. M., Jeong, K., Choi, K., Choi, M., & Noh, J. H. (2021). Intact 2D/3D halide junction perovskite solar cells via solid−phase in−plane growth. Nature Energy, 6(1), 63−71.

[21] Meng, L., You, J., & Yang, Y. (2018). Addressing the stability issue of perovskite solar cells for commercial applications. Nature communications, 9(1), 1−4.

[22] Saliba, M., Correa−Baena, J. P., Wolff, C. M., Stolterfoht, M., Phung, N., Albrecht, S., ... & Abate, A. (2018). How to Make over 20% Efficient Perovskite Solar Cells in Regular (n–i–p) and Inverted (p–i–n) Architectures. Chemistry of Materials, 30(13), 4193−4201.

[23] Deng, Y., Wang, Q., Yuan, Y., & Huang, J. (2015). Vividly colorful hybrid perovskite solar cells by doctor−blade coating with perovskite photonic nanostructures. Materials Horizons, 2(6), 578−583.

[24] Chiang, C. H., Lin, J. W., & Wu, C. G. (2016). One-step fabrication of a mixed-halide perovskite film for a high-efficiency inverted solar cell and module. Journal of Materials Chemistry A, 4(35), 13525-13533.

[25] Köster, U. (1978). Crystallization of amorphous silicon films. Physica status solidi (a), 48(2), 313-321.

[26] Niu, G., Guo, X., & Wang, L. (2015). Review of recent progress in chemical stability of perovskite solar cells. Journal of Materials Chemistry A, 3(17), 8970-8980.

[27] Mehmood, U., Al-Ahmed, A., Afzaal, M., Al-Sulaiman, F. A., & Daud, M. (2017). Recent progress and remaining challenges in organometallic halides based perovskite solar cells. Renewable and Sustainable Energy Reviews, 78, 1-14.

[28] Kosasih, F. U., & Ducati, C. (2018). Characterising degradation of perovskite solar cells through in-situ and operando electron microscopy. Nano Energy, 47, 243-256.

[29] Asghar, M. I., Zhang, J., Wang, H., & Lund, P. D. (2017). Device stability of perovskite solar cells-A review. Renewable and Sustainable Energy Reviews, 77, 131-146.

[30] Pisoni, A., Jacimovic, J., Barisic, O. S., Spina, M., Gaál, R., Forró, L., & Horváth, E. (2014). Ultra-low thermal conductivity in organic-inorganic hybrid perovskite CH3NH3PbI3. The journal of physical

chemistry letters, 5(14), 2488-2492.

[31] Asghar, M. I., Zhang, J., Wang, H., & Lund, P. D. (2017). Device stability of perovskite solar cells-A review. Renewable and Sustainable Energy Reviews, 77, 131-146.

[32] Jiang, Y., Qiu, L., Juarez-Perez, E. J., Ono, L. K., Hu, Z., Liu, Z., ... & Qi, Y. (2019). Reduction of lead leakage from damaged lead halide perovskite solar modules using self-healing polymer-based encapsulation. Nature Energy, 4(7), 585-593.

[33] Wang, C., Zhang, Y., Gu, F., Zhao, Z., Li, H., Jiang, H., ... & Liu, Z. (2021). Illumination durability and high-efficiency Sn-based perovskite solar cell under coordinated control of phenylhydrazine and halogen ions. Matter, 4(2), 709-721.

Chapter 2. SIG (Solid-state Inplane Growth) process

2.1. Introduction

The application of 3D halide materials to PSCs results in poor stability due to their hydrophilic properties. [1,2] To improve the stability of 3D halide perovskite, various approaches have been used, either by grain boundary control [3] or by hydrophobically tuning the thin film surface of the perovskite. Recent research on PSC has shifted interest from the use of 3D perovskite to 2D halide perovskite material because of its stability, and how to use it as a capping layer is mainly studied. [4] The 2D capping layer provides many interesting features with improved stability, but it is very difficult to create the intact 2D:3D structure, making it very difficult to study the mechanism. I devised a SIG process that removes the damage to the 3D perovskite surface by solvent, and analyze the properties of the new bilayer thin film.

2.1.1. Existing technology

The introduction of large organic cations that do not fit into the three-dimensional perovskite structure of the perovskite film can have various effects on the film composition and properties depending on the method. The factors are the type, size and specific properties of such molecules such as density and deposition conditions. Combinations occur in many cases, and three main categories have been identified. There are four methods: 1) mixed 2D/3D perovskite phase formation, 2) 2D capping layer formation (2D:3D structure) 3) grain boundary passivation.

Among them, a strategy of forming a Ruddlesden-Popper 2D perovskite layer on the surface of a 3D light absorbing perovskite layer has recently been attracting attention. This strategy can form 2D:3D heterojunctions while reducing surface defects by surface passivation. 2D:3D junctions must be carefully designed based on photoelectric properties such as bandgap and work function. However, a process using a solution state precursor forms an unidentified and unintentional quasi-2D perovsktie, [10] which prevents the design of an appropriate electric field distribution at the junction. This is because the solution process is based on the reaction of 2D precursor (A*I) and 3D ($APbI_3$) on top dissolved in solvent.

This reaction will produce the quasi-2D phase $(A*)_2A_{n-1}Pb_nI_{3n+1}$ (1 < n < ∞) leaving behind (AI).[11] This implies an unspecified state, which means that existing solution processes struggle to form a clear 2D:3D junction to form an optimal electric field.

Existing solution process:

$$2(A*I)+n(APbI_3) \rightarrow (A*)_2A_{n-1}Pb_nI_{3n+1}(1 \leq n < \infty)+(AI)$$
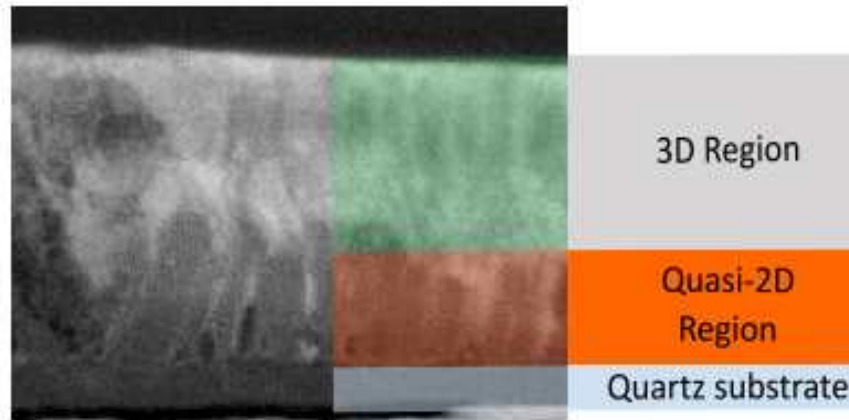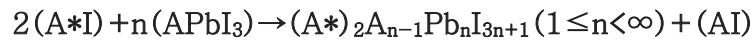
Figure 4. Cross sectional SEM image of 2D:3D junction precessed by existing solution process. This image is adopted from reference[18].

2.2. SIG process

2.2.1. SIG-2D:3D structure fabrication

Note: This chapter is reproduced from the work I co-authored with Seungmin Lee published in Nature Energy 6 (1), 63-71.

The 2D:3D structure in the N-I-P device is to newly form a 2D perovskite on the already formed 3D. Therefore, the selection of the solution is very limited, resulting in a number of problems arising from the use of the solution, such as forming a 2D perovskite layer in a poor state or destroying the 3D layer below. Therefore, I devised a SIG process that separates the process of forming 2D and the process of forming 2D:3D junction with researcher Seungmin Lee of AECMD lab. For the SIG process, $2D(BA)_2PbI_4$ and $3D(FAPbI_3)_{0.95}(MAPbBr_3)_{0.05}$ (where FA is formamide and MA is methylammonium) films were prepared on the substrate. For instructions, see reference.[12]

Figure 5 is a schematic diagram of the SIG process procedure. A solid 2D film is laminated on top of the 3D film so that the surface is in contact. Pressure and heat are then applied perpendicularly to the bonding surface, inducing the supply of 2D perovskite from the laminated solid 2D precursor film to the top of the 3D film. The two-dimensional seed is formed in the early stages and gradually grows in-plane direction on the 3D film to become a new 2D film. After a

certain process time, the original 2D solid precursor is isolated and an intact 2D/3D double layer is finally formed. The reaction means the formation of an intact 2D perovskite thin film, following the following formula:

SIG process:

$$(A*)_2PbI_4+(APbI_3)\rightarrow(A*)_2PbI_4/(APbI_3)$$
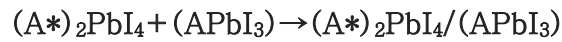
The experimental results indicate that the three elements of heat and pressure time influence the formation of the thin film in the SIG process. Set notation for interpretation of results. All SIG processes were performed at 60 MPa, except for experiments that examined the effect of pressure. Temperature conditions are shown after the SIG.

Figure 6 shows the scanning electron microscope (SEM) plane image of the SIG60 treated film as a function of the processing time. This tells you how the 2D layer is formed over time. The SEM image of the SIG60-2 min case shows the initial state of the small seed morphology appearing on the 3D surface. The seed grows and gradually fills the 3D surface. The material was sufficiently covered on the 3D surface in about 10 minutes. The X-ray diffraction (XRD) results for the same SIG film support that the observed material is

$(BA)_2PbI_4$. Only one new peak appears at 6.4° from 2 min to 10 min, increasing gradually over time. (Figure 7) This peak corresponds to the (002) plane and corresponds to the peak of the original precursor 2D film. [13] This indicates that the new 2D film was provided from the original solid precursor 2D film.

Pressure is involved in the formation of early seeds by helping close contact between the two films. I observed that 2D perovskite attachment did not occur on the 3D surface in the absence of pressure (Figure 8). Pressure also has the effect of promoting in-plane growth of the 2D layer. As Figure 8 shows the 2D crystals are still in the process of formation at 20 MPa while at 60 MPa they are almost completely flattened.

Temperature also has the greatest impact on crystal formation and growth. Figure 9 shows the thickness of the 2D film for SIG30 and SIG60 over time. It can be seen that even if the processing time is increased up to 720 min, the thickness in the out-of-plane direction hardly increases over time. This suggests that the seed grows in the in-plane direction while the height of the initial seed remains over time, possibly due to the 2D material properties. As a result, a thicker 2D layer is created at higher temperatures, as shown in Figure 10. Also XRD data from each condition shows there is no unidentified material excepting N=1 state 2D perovskite and the peak also get

2 7

higher according to temperature. (Figure 11)

According to the nucleation-growth theory, crystals from early precursors can be described as differences in Gibbs free energy due to surface area and volume changes of newly formed crystals. [14] However, the SIG process does not produce new crystals using solidified precursors. Therefore, we assume that there will be no free energy change due to volume change, but surface area change still occurs when the original crystal surrounded by 2D precursor film changes from 3D surface to 2D seed. The heat supplied determines the progress of the reaction, balanced by the energy change due to the newly formed surface area of the seed and the difference in the increased free energy. As a result, the temperature can determine the initial seed height and final thickness of the SIG-2D film. We also showed that the seeds did not grow into 2D films at 20 °C, whereas they succeeded at 30 °C (Figure 12), indicating that sufficient thermal energy was needed for in-plane growth.
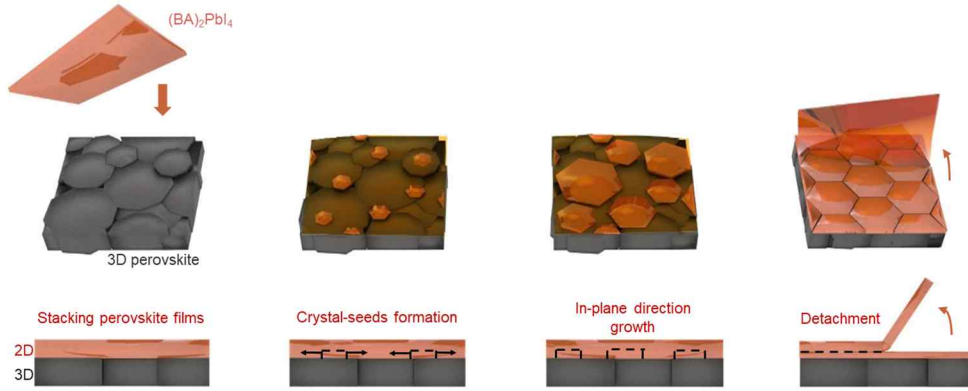
Figure 5. Top-view and cross-sectional sketches of the manufacturing of a $(BA)_2PbI_4$ film on a 3D perovskite substrate via the SIG method. The formation of crystal seeds and the in-plane grain growth are indicated with black dashed lines and black arrows, respectively, in the cross-sectional representation of the perovskite layer. This image is adopted from reference[12].
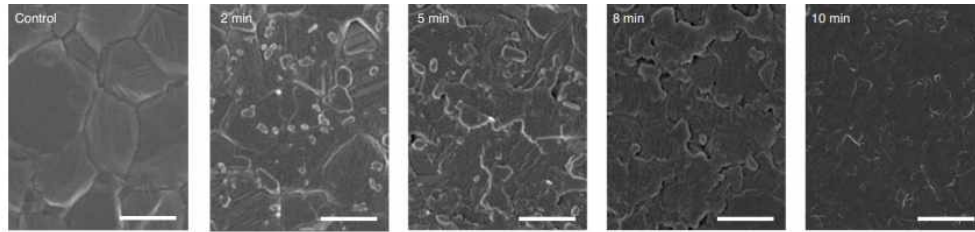
Figure 6. Top surface SEM images of the 3D:2D perovskite in SIG process.
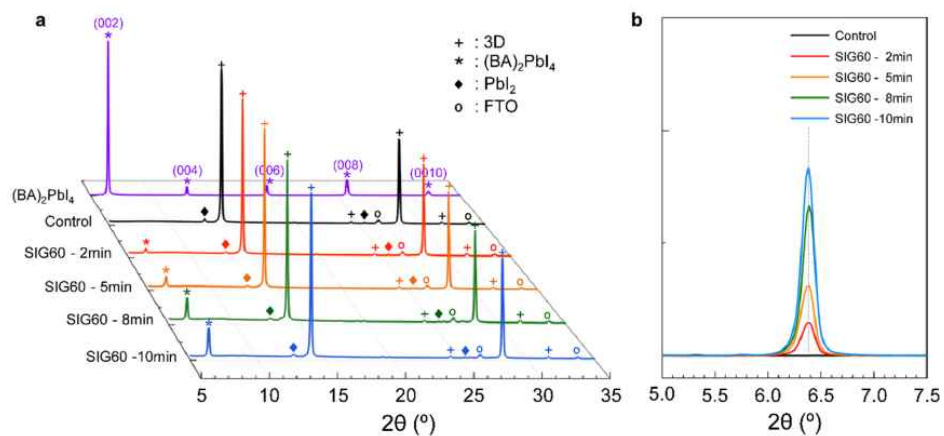
Figure 7. Time-dependent X-ray diffraction patterns of SIG60 films.
a, XRD patterns of SIG60 films according to the SIG process time. b,
Trend of the $(BA)_2PbI_4(002)$ peak over time. As the time of the SIG
method increased, the intensity of the $(BA)2PbI4$ peak was enhanced.
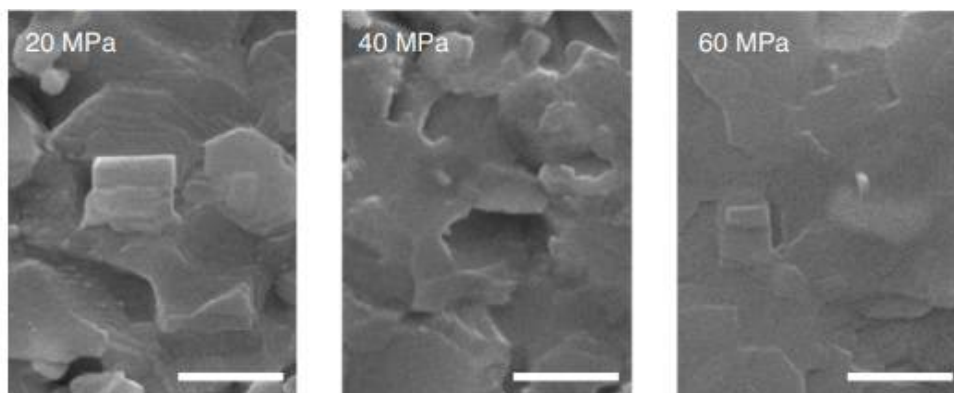
Figure 8. Top surface SEM images of SIG60-processed 2D/3D films
after 10 min at 20 MPa (g), 40 MPa (h) and 60 Mpa
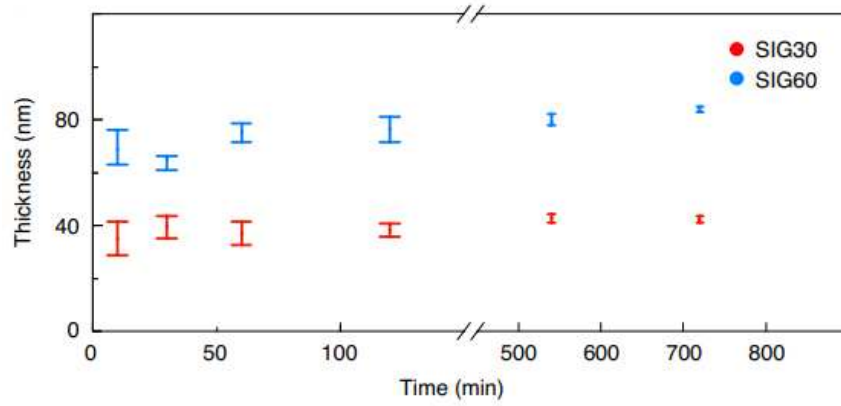
Figure 9. The thickness distribution of the grown $(BA)_2PbI_4$ accretion with processing time. Five samples were used in every case to measure the change in thickness over time under SIG30, whereas six samples were used for SIG60. Error bars show the lower and upper thicknesses of $(BA)_2PbI_4$ at each condition.
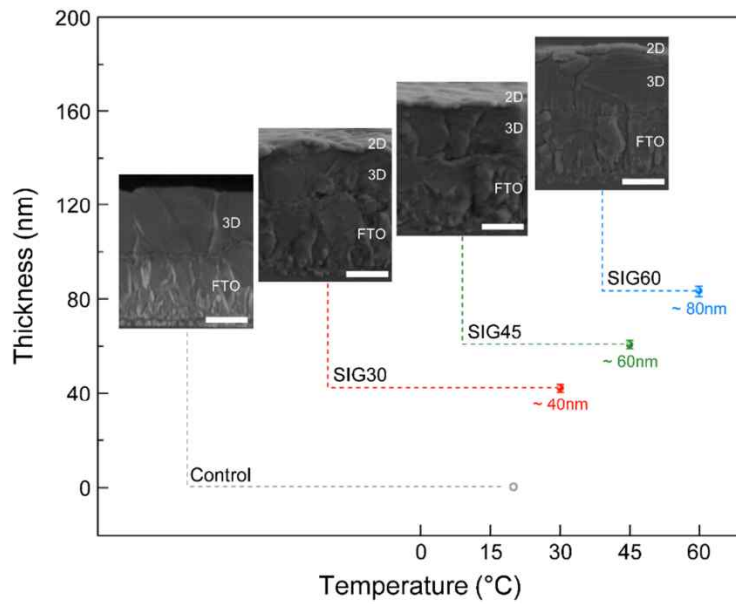
Figure 10. SIG$-(BA)_2PbI_4$ thickness as a function of SIG temperature. The thickness of $(BA)_2PbI_4$ fabricated at each SIG temperature. All thicknesses of $(BA)_2PbI_4$ were observed through SEM images. Inserts are representative images of each SIG film. Error bars show the lower and upper thicknesses of $(BA)_2PbI_4$ at each SIG temperature. All scale bars: 500 nm.
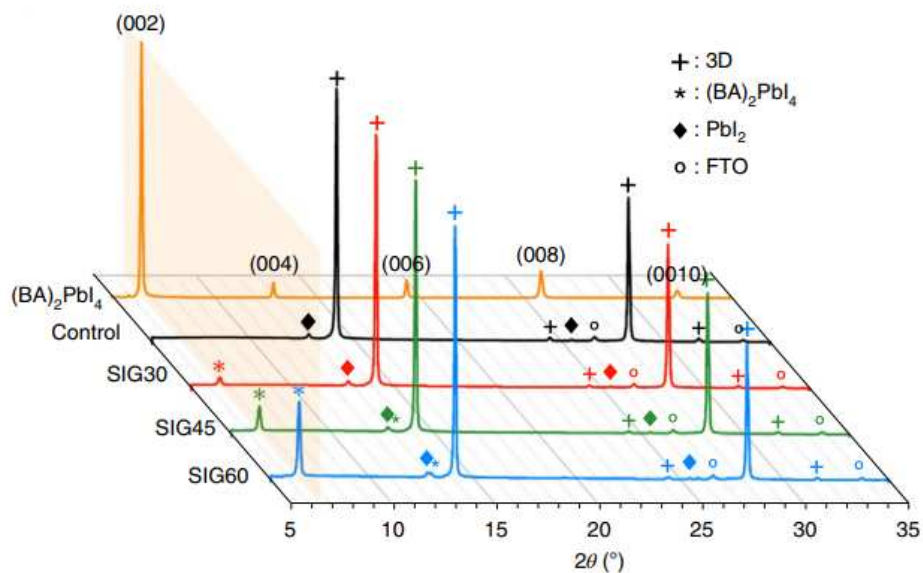
Figure 11. X-ray diffraction patterns of the control film (3D perovskite only), 2D/3D films developed by the SIG process under different temperature conditions, and a pure 2D perovskite film (n= 1, (BA)₂PbI₄. The orange shading indicates 6.4°.
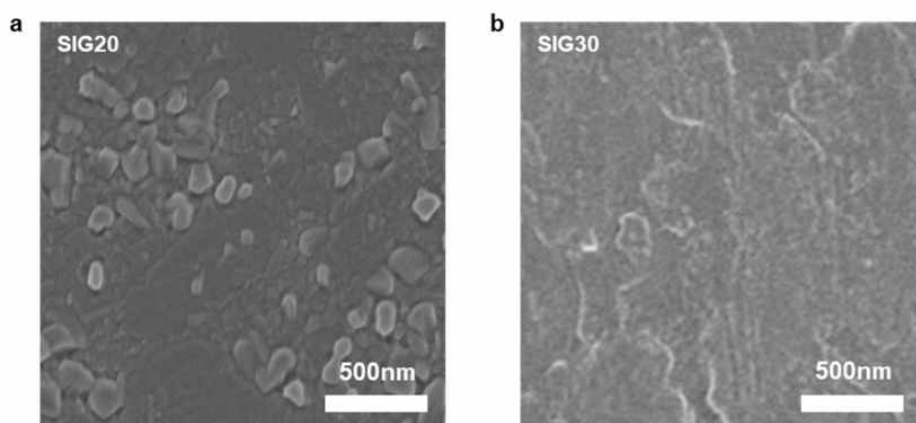
Figure 12. Lower temperature limit of SIG-(BA)₂PbI₄ on the surface of the 3D film. a-b. SEM images of the SIG film surface after 12 h under a 60 MPa pressure at 20°C (a) and 30°C (b).

2.2.2. Property of SIG-2D:3D perovskite heterojunction

Figure 11 shows the XRD results for the control 3D film, the original 2D $(BA)_2PbI_4$ film and the SIG-2D/3D bilayer film formed at different temperatures. All SIG films show typical peaks present at $6.4°$ and have no other unknown peaks. The SIG-2D film formed by the SIG process shows a small FWHM(full width at half maximum) value of $\sim0.167°$ over 3D. (Table 1) Contains an instrumental broadening value of $0.061°$ that is appropriately estimated at the location. The FWHM value of the SIG-2D film is significantly smaller than the FWHM value reported above $0.50°$ for the (002) peak of the 2D layer obtained in the existing solution process. [15,16] This supports the SIG process along with HRTEM data (Figure 13) to form a tens of nanometer thick upper layer containing a high crystallinity pure 2D phase on top of the 3D layer. This is also valid for pure $FAPbI_3$ and $MAPbI_3$ perovskites (Figure 14).

Figure 15 shows the time-resolved photoluminance (TRPL) attenuation curve of the control 3D and SIG films. The primary decay associated with trap-assisted nonradiative recombination can be identified by fitting exponential decay within the axial tail region. [17] The fitting results are shown in Figure 16, respectively. The obtained recombination constants and lifetime are summarized in Table 2. The

SIG process improves the life of the primary recombination to approximately 1.1 μs (at 0.2 μs control) regardless of the processing temperature. This means that the SIG process reduces trap-assisted nonradioactive recombination and that the processing temperature does not affect carrier life. The reduction of surface defects appears to be independent of the SIG-2D film thickness due to the constant contact area between 2D and 3D materials.

The change in average carrier life over processing time is also shown by the life mapping in Figure 17. You can see that the short-lived blue area gradually switches to the long-lived green area, which means the area covered by 2D. The result of two minutes indicates an area partially covered by the seed. After 10 minutes, the 2D film covered all areas through in-plane growth. TRPL results show that the 2D film successfully immobilized the surface of the 3D film through the SIG process. As we will discuss the device performance again later, it should be noted that the improved life of 1.1 μs is insufficient to achieve a high open circuit voltage (VOC = 1.185 V) for SIG devices in this study. The fact that VOC increases as the SIG-2D thickness increases (despite similar life expectancy of 1.1 μs) considers the contribution of other factors to VOC improvement, which is estimated to be the effect of the p-p type heterojunction discussed earlier.

Meanwhile, the SIG process does not react with the three dimensional surface, producing a clear and crystalline two-dimensional (n = 1) perovskite on the three-dimensional perovskite, suggesting that the thickness of the 2D layer can be controlled by the iterative process. In fact, we observed that a uniform and intact 2D/3D double layer was formed across the entire surface of the SIG film in slightly tilted cross-sectional SEM images (Figure 18). The SIG now allows the electric field to be designed. SIG and solution processes were performed twice in a row to assess the potential of electric field design to ensure proper 2D thickness. Figure 19a-c shows the GIWAXS (grazing incident wide-angle X-ray scattering) image of the contrasting 3D film, solution treated (2 times) 2D/3D film and SIG60 treated (2 times) 2D/3D film. As expected, the solution-treated film exhibits a wide peak, indicating the generation of quasi 2D with undefined phases (Figure 19b). In contrast, our SIG-treated film consistently shows a single sharp peak corresponding to pure $(BA)_2PbI_4$ (Figure 19c). This means that the target 2D material can grow on the 3D surface to the desired thickness using repetition of the SIG process (Table 3).

Film type	Film structure	Peak position (2θ)	FWHM (°)
$(BA)_2PbI_4$	ITO/2D	6.41	0.105
SIG30	FTO/3D:SIG-2D	6.38	0.167
SIG45	FTO/3D:SIG-2D	6.38	0.153
SIG60	FTO/3D:SIG-2D	6.39	0.152

Table 1. Position of the (002) peak of the (BA)2PbI4 films and its FWHM in XRD patterns. The XRD pattern of a pure (BA)2PbI4 film fabricated by spin coating on ITO showed an FWHM of 0.105° for the (002) peak. SIG films with (BA)2PbI4, even for different temperature conditions (30℃, 45℃, and 60℃), showed FWHMs of 0.152 ° to 0.167 ° at the position corresponding to the (002) peak of pure (BA)2PbI4. The small FWHM of 0.15° means that the SIG process can induce a highly crystalline (BA)2PbI4 film on the 3D perovskite surface compared to conventional processes.
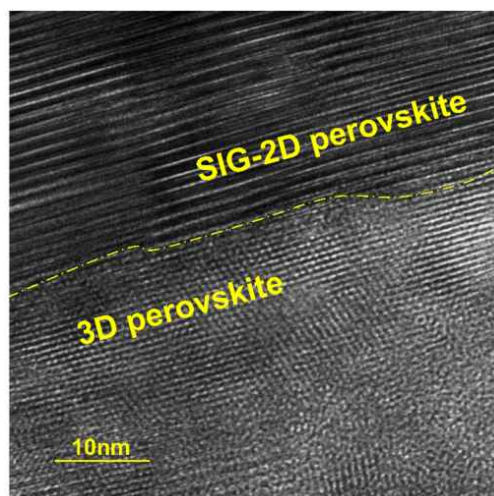
Figure 13. High-resolution transmission electron microscopy image at the junction between the 3D material and SIG-(BA)2PbI4 of the SIG60 film.
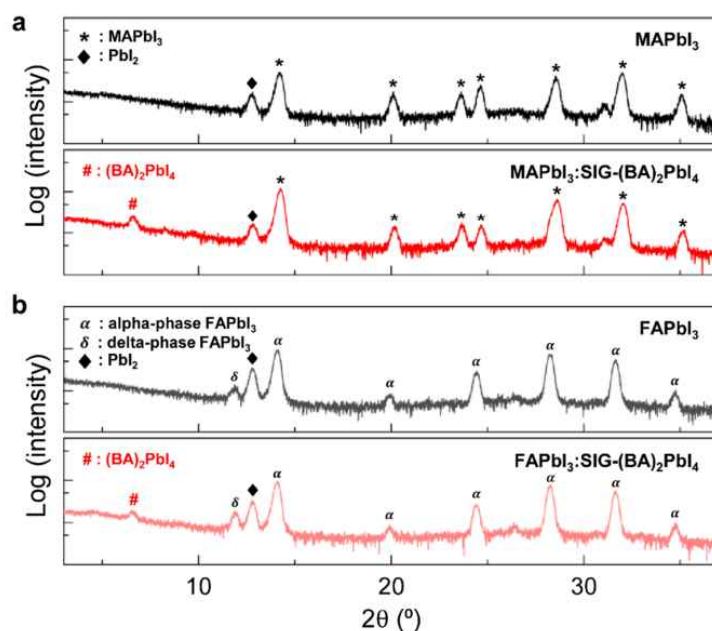
Figure 14. XRD patterns of 3D and 3D:SIG-(BA)2PbI4 in compliance with the 3D perovskite composition. Similar to (FAPbI3)0.95(MAPbBr3)0.05, after the SIG process, a typical (BA)2PbI4 peak was found near 6.4° in either the (a) MAPbI3 or (b) FAPbI3 composition.

3 7
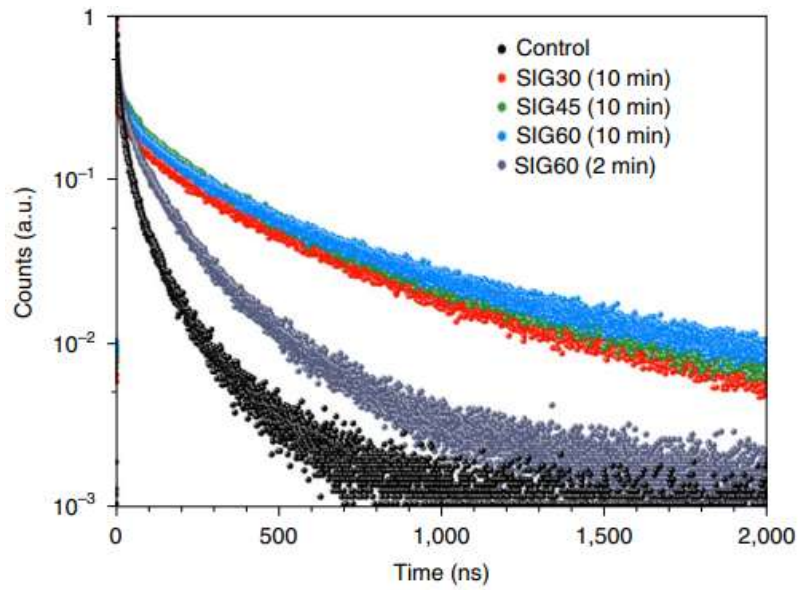
Figure 15. Time-resolved photoluminescence decay curves of the control and SIG-processed 2D/3D films after excitation at 800 nm and 0.5 MHz.
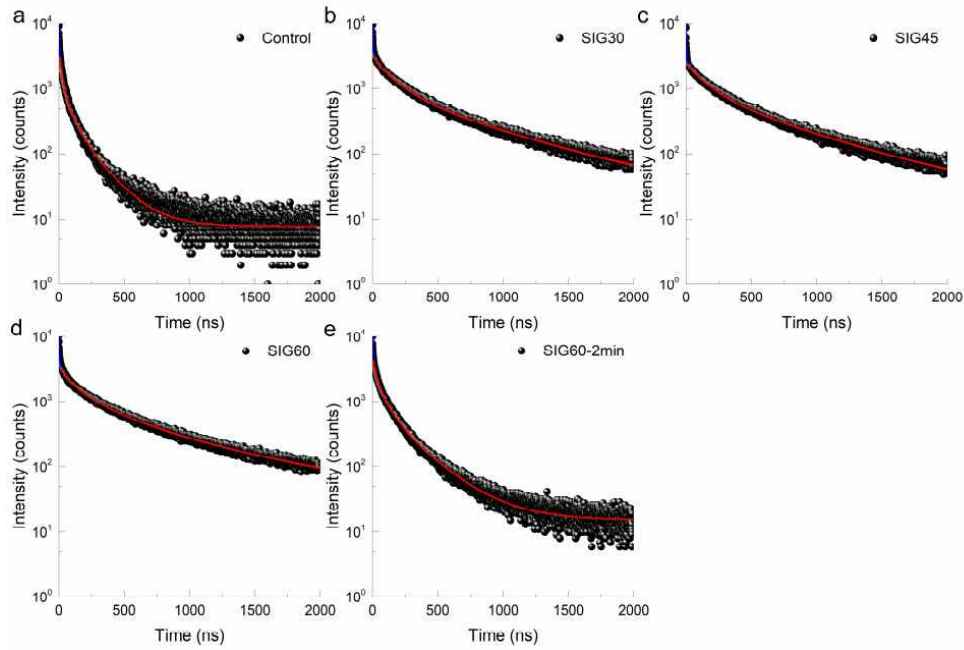
Figure 16. SIG method effect related to the trap-assisted lifetime in TRPL. a-e, PL decay plots of the control film and SIG films. To identify the first-order recombination lifetime, mono-exponential fitting was used to fit the exponential decay within the PL tail region.

Condition	First-order		Second-order	Reduced Chi-square
	Lifetime (ns)	k_1 (1/s)	k_2 (cm^3/s)	
Control	202.89	4.93×10^6	3.18×10^{-10}	1.120
SIG30	1052.77	0.95×10^6	5.35×10^{-11}	1.214
SIG45	1005.35	1.00×10^6	4.17×10^{-11}	1.199
SIG60	1114.22	0.90×10^6	4.79×10^{-11}	1.196
SIG60 2 min	267.48	3.74×10^6	2.09×10^{-10}	1.101

Table 2. Recombination constant fitted from the PL decay for the control and SIG process conditions.
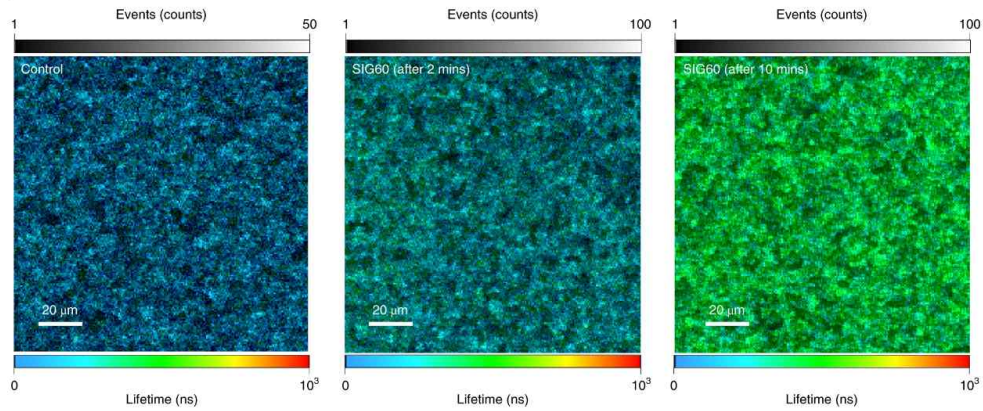
Figure 17. Average lifetime mapping images of the 3D perovskite film and 2D/3D films after 2 min and 10 min of processing under SIG60. The colour–scale bars indicate average carrier lifetime whereas the greyscale bars indicate event counts.
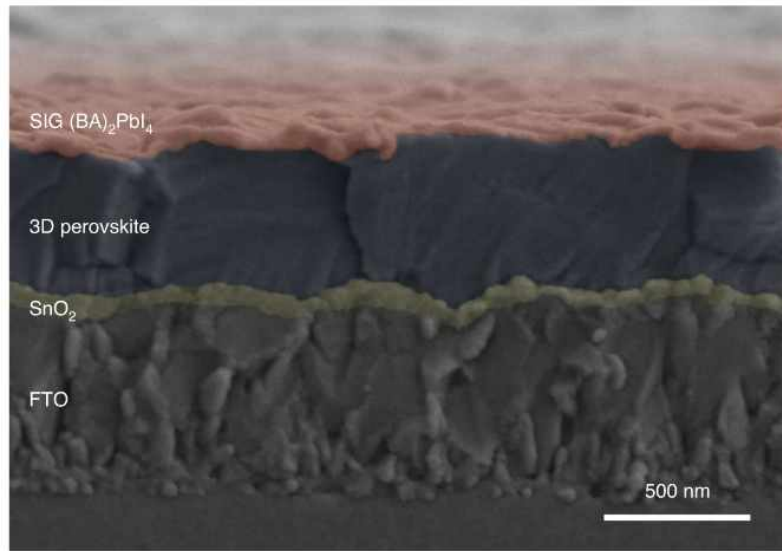
Figure 18. A cross−sectional SEM image of the SIG−processed 2D/3D device.
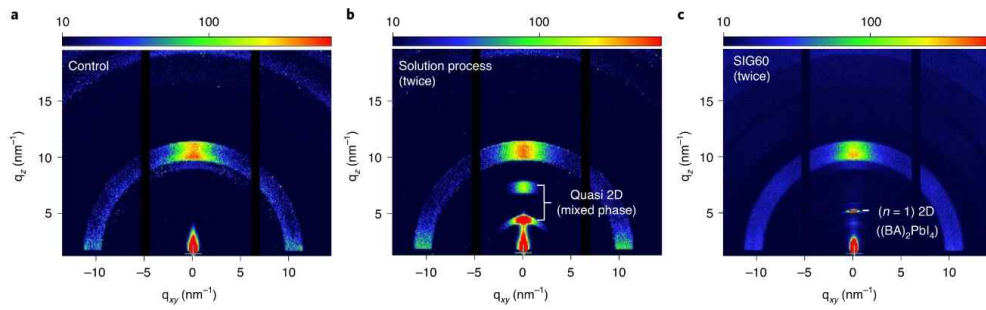
Figure 19. GIWAXS patterns of the 3D perovskite film (control) (a) and 2D/3D perovskites made by two cycles of the solution (b) and SIG (c) processes. q is the scattering vector. The colour−scale bars indicate intensity.

	2D perovskite precursor solution post-deposition	2D perovskite Solid-phase In-plane Growth (SIG) process
State of precursor	Liquid	Solid
Formation mechanism	$BAI_{(aq)} + \Delta_1 \rightarrow (BA)_2PbI_{4\,(s)} + \Delta_2$ Δ_1: material from 3D perovskite surface Δ_2: material of uncertain composition	$(BA)_2PbI_{4\,(s)} \rightarrow (BA)_2PbI_{4\,(s)}$
Strengths	Thin layer processible Surface passivation	Identified compartmental film Perfect stoichiometry Multiple layer processible Easy thickness control
After process iteration	Fusion with 3D perovskite substrate	Intact multiple layer film formation with the desired thickness

liquid-state deposition   solid-state deposition
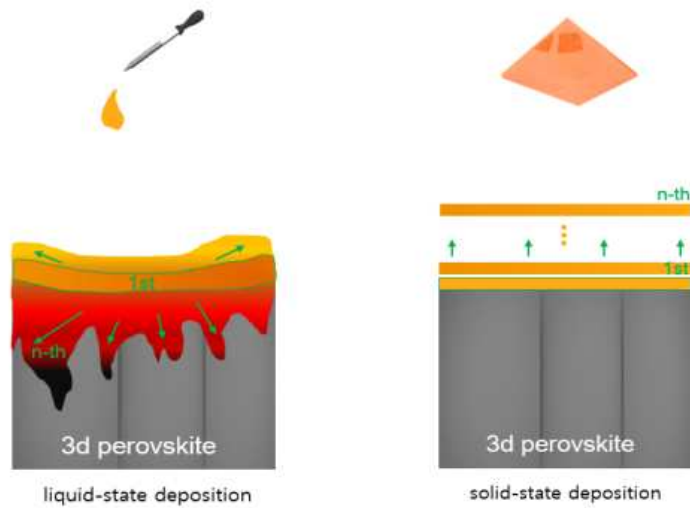
Table 3. Comparison of SIG and solution process methods for fabricating a 2D perovskite layer on a 3D perovskite.

4 1

2.2.3. Mechanism of SIG

Note: This chapter is reproduced from the work I co-authored with Wonjin Cho.

The SIG process is currently based on the reaction on organic-inorganic halide, but it can be applied to much more diverse places based on the study of each interface participating in the reaction. Above all, it is important for us to understand the reaction in which the two 'solid-state' interfaces participate in the SIG process. This reaction is related to the solidified 2D perovskite and 3D perovskite and the energy supplied after these interfaces meet.

The research we need is for each interface, 2D perovskite and 3D perovskite, respectively. The SIG reaction is a reaction in which the combination of an unstable and stable surface creates two stable surfaces, and it is obvious that the reaction is spontaneous. (Figure 20) However, in terms of crystal growth, we need a deeper understanding. From the classical crystal growth point of view, crystal seeds have gibb's energy values related to volume and area, respectively, and these values change as the effective radius increases. When the influence of those values acts in a direction where the change in gibb's energy of the final reaction becomes negative, the reaction is spontaneous and a seed is found with the size of the critical radius at that point. This is the initial very small

seed found in Figure.6, and this seed gradually grows in the direction of covering the surface according to the property that 2D perovskite grows relatively better in the plane direction after discovery. The shape actually grows in a more irregular form rather than maintaining the crystal plane, which is thought to be because the heat supply in the solid phase process is growing relatively fast for some reason. Each interface grows in a preferential direction rather than keeping the crystal plane shape while observing the Gibb-Curie law. This is why many analyzes are difficult at the current level. In fact, theoretically, the supplied energy should appear in a direction that minimizes the increase in energy of each crystal plane formed per volume increase as the seed grows, and in this case, of course, a very neat 2D thin film can be formed. For this process, we can first obtain the surface energy of each interface from a single crystal and predict which interface will prefer to grow. And conversely, you can predict how much energy supply is most appropriate. Eventually, surface analysis of 2D single crystals can give hints about this. In the case of growing other materials, the same is expected to be applied.

It is also necessary to understand the other interface, the 3D perovskite interface. The 3D perovskite supplying surface energy does not change during the growth reaction but provides the so-called basic energy state of the reaction surface. Of course,

depending on the degree of interaction with 2D, changes in directions that we do not expect are expected to be possible. As already shown in the figure, it was confirmed that the mechanism of SIG appeared the same in the experiment with different 3D perovskites. (Figure 14) However, it can be expected that there is a change in the result depending on the type and state of the 3D peorvskite corresponding to the reactant. Together with researcher Cho Wonjin, I am studying the changes in SIG growth patterns according to various 3D conditions. In particular, the Classical nucleation-growth theory deals with seeds growing in solution, so it is inevitable to overlook the specificity of the reaction that can only appear in the solid phase, so research is being conducted on the contribution of the energy of the solid surface to the reaction.

Finally, it is necessary to analyze the contribution of the factors affecting the defects of the two interfaces. In previous experiments, the factors of sig affected by heat and pressure time have been analyzed. However, although each element is a thermodynamically representative factor, its properties are slightly different. In particular, in the case of pressure, the structure of the crystal itself changes when it reaches a certain area, but in the area below it, it supplies appropriate energy without damaging the crystal. In the case of basic SIG, it is known that a pressure of about 60 Mpa at a

temperature of about 60 ℃ is appropriate for seed growth. The special effects of moderate pressures on solid-state processes are also being studied. We will be able to use SIG more skillfully based on the study of the reactants that participate in these reactions and the factors that influence their outcome.
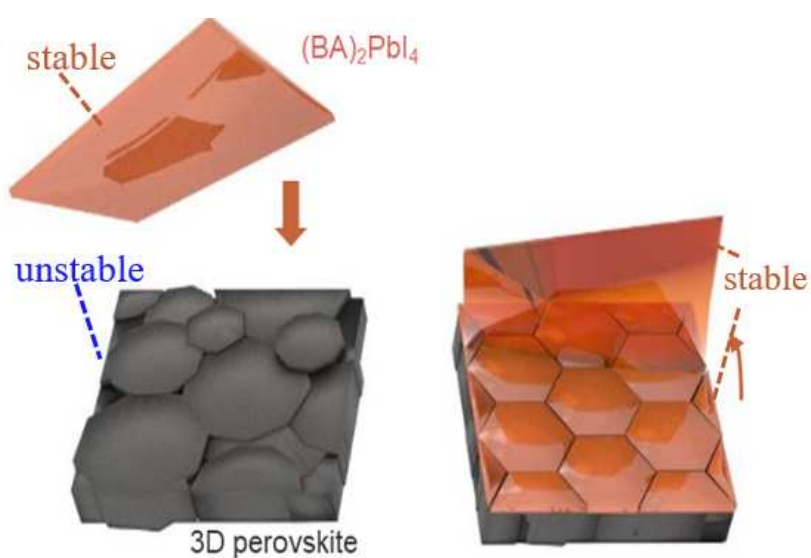
Figure 20. Energy states of reactants and products in the SIG process

2.2.4. Technology potential

The SIG process of repeatable process, the ability to form a very clean and healthy 2D:3D bilayer, has tremendous potential. Figure 21 shows the direction of future develpoment potential of SIG technology. First of all, we can produce various 2D:3D structures that have changed 2D types by incorporating the diversity of 2D materials. This can create structures with different photoelectric properties, ranging from crystallographic distinctions such as ACI(alternating cations in the interlayer space), RP(ruddlesden popper perovskite), and DJ(dion jacobson)to organic chain changes. As already confirmed, the SIG process is applicable to other perovskite thin films. This means that it can be extended from an organic material to an organic material surface. Stacking loops based on iterative processes can create larger extensions. Multi-layered multi-2D:3D structure can selectively give various properties or act as an encapsulator or photo collector helper using chemical and optical characteristic differences. Using the properties of halide-based perovskites, it can also be used as a nano process to process very thin layers by using fusions on each perov surface or by thin-film exfoliation. With only a few properties of 2D perovskite, this tremendous technological potential can be realized in the near future.
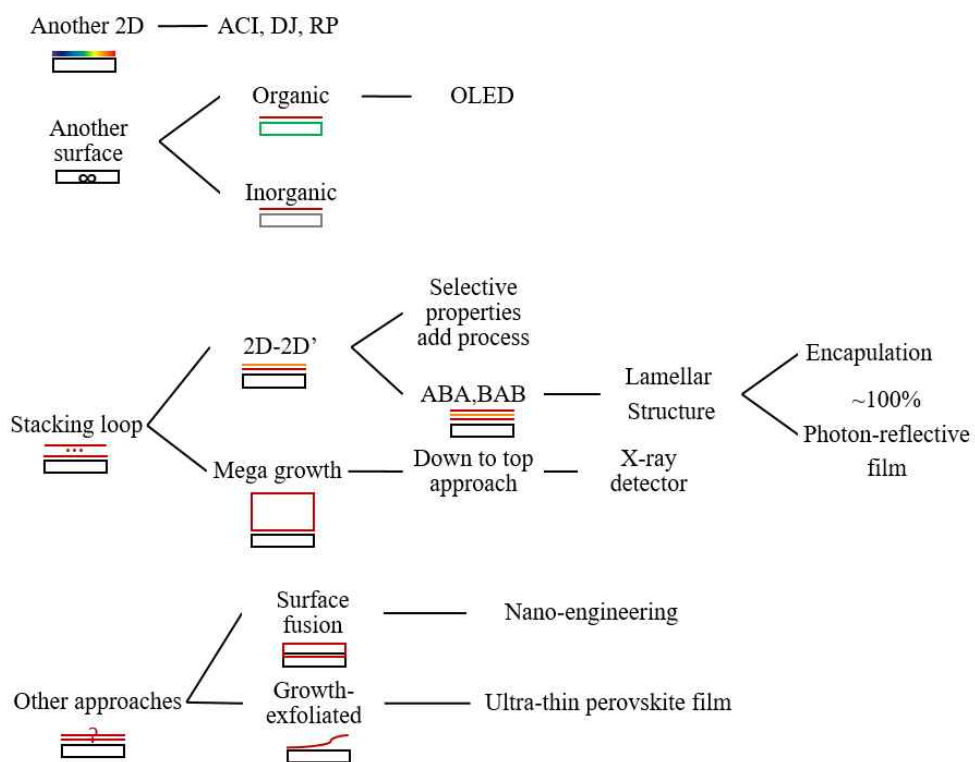
Figure 21. Technology deployment branch model of SIG process.

2.4. Conclusion

I developed a SIG strategy that enables the formation of intact 2D:3d films. An improvement in PSC can be expected in terms of intact 2D:3D halide bonding efficiency and stability, which demonstrates remarkable performance. This growth is based on a classic seed-growth approach. Since it is possible to repeat the process and define the state of each material layer, it becomes a base technology that can design local electric field distribution at stable joints, and based on this property, it is possible to access various materials from nano-scale processes.

2.5. References

[1] Shi, D., Adinolfi, V., Comin, R., Yuan, M., Alarousu, E., Buin, A., ... & Bakr, O. M. (2015). Low trap-state density and long carrier diffusion in organolead trihalide perovskite single crystals. Science, 347(6221), 519-522.

[2] Zhang, J., Meng, Z., Guo, D., Zou, H., Yu, J., & Fan, K. (2018). Hole-conductor-free perovskite solar cells prepared with carbon counter electrode. Applied Surface Science, 430, 531-538.

[3] Meng, Z., Guo, D., Yu, J., & Fan, K. (2018). Investigation of Al2O3 and ZrO2 spacer layers for fully printable and hole-conductor-free mesoscopic perovskite solar cells. Applied Surface Science, 430, 632-638.

[4] Li, G., Zhang, T., Guo, N., Xu, F., Qian, X., & Zhao, Y. (2016). Ion-Exchange-Induced 2D-3D Conversion of HMA1− xFAxPbI3Cl Perovskite into a High-Quality MA1− xFAxPbI3 Perovskite. Angewandte Chemie International Edition, 55(43), 13460-13464.

[5] Chen, Y., Lei, Y., Li, Y., Yu, Y., Cai, J., Chiu, M. H., ... & Xu, S. (2020). Strain engineering and epitaxial stabilization of halide perovskites. Nature, 577(7789), 209-215.

[6] Jung, E. H., Jeon, N. J., Park, E. Y., Moon, C. S., Shin, T. J., Yang, T. Y., ... & Seo, J. (2019). Efficient, stable and scalable perovskite solar cells using poly (3-hexylthiophene). Nature, 567(7749), 511-

515.

[7] Kim, H., Lee, S. U., Lee, D. Y., Paik, M. J., Na, H., Lee, J., & Seok, S. I. (2019). Optimal interfacial engineering with different length of alkylammonium halide for efficient and stable perovskite solar cells. Advanced Energy Materials, 9(47), 1902740.

[8] Gunawan, O., Pae, S. R., Bishop, D. M., Virgus, Y., Noh, J. H., Jeon, N. J., ... & Shin, B. (2019). Carrier-resolved photo-Hall effect. Nature, 575(7781), 151-155.

[9] Zhang, F., Ullrich, F., Silver, S., Kerner, R. A., Rand, B. P., & Kahn, A. (2019). Complexities of contact potential difference measurements on metal halide perovskite surfaces. The Journal of Physical Chemistry Letters, 10(4), 890-896.

[10] Cho, Y., Soufiani, A. M., Yun, J. S., Kim, J., Lee, D. S., Seidel, J., ... & Ho-Baillie, A. W. (2018). Mixed 3D-2D passivation treatment for mixed-cation lead mixed-halide perovskite solar cells for higher efficiency and better stability. Advanced Energy Materials, 8(20), 1703392.

[11] Tai, M., Zhou, Y., Yin, X., Han, J., Zhang, Q., Zhou, Y., & Lin, H. (2019). In situ formation of a 2D/3D heterostructure for efficient and stable CsPbI 2 Br solar cells. Journal of Materials Chemistry A, 7(39), 22675-22682.

[12] Jang, Y. W., Lee, S., Yeom, K. M., Jeong, K., Choi, K., Choi, M.,

& Noh, J. H. (2021). Intact 2D/3D halide junction perovskite solar cells via solid-phase in-plane growth. Nature Energy, 6(1), 63-71.

[13] Cao, D. H., Stoumpos, C. C., Farha, O. K., Hupp, J. T., & Kanatzidis, M. G. (2015). 2D homologous perovskites as light-absorbing materials for solar cell applications. Journal of the American Chemical Society, 137(24), 7843-7850.

[14] Porter, D. A., & Easterling, K. E. (2009). Phase transformations in metals and alloys (revised reprint). CRC press.

[15] Wang, Z., Lin, Q., Chmiel, F. P., Sakai, N., Herz, L. M., & Snaith, H. J. (2017). Efficient ambient-air-stable solar cells with 2D-3D heterostructured butylammonium-caesium-formamidinium lead halide perovskites. Nature Energy, 2(9), 1-10.

[16] Lin, Y., Fang, Y., Zhao, J., Shao, Y., Stuard, S. J., Nahid, M. M., ... & Huang, J. (2019). Unveiling the operation mechanism of layered perovskite solar cells. Nature communications, 10(1), 1-11.

[17] Zhao, B., Bai, S., Kim, V., Lamboll, R., Shivanna, R., Auras, F., ... & Di, D. (2018). High-efficiency perovskite-polymer bulk heterostructure light-emitting diodes. Nature Photonics, 12(12), 783-789.

[18] Liu, B., Long, M., Cai, M., Ding, L., & Yang, J. (2019). Interfacial charge behavior modulation in 2D/3D perovskite heterostructure for potential high-performance solar cells. Nano Energy, 59, 715-720.

Chapter 3. Photo-physical Approach for High efficiency

3.1. Introduction

The high power conversion efficiency of solar cells enables the widespread use of renewable solar energy. We can predict the upper bound of solar cell efficiency based on the radiation balance argument based on the Shockley-Queisser (SQ) theory [1,2] Among the considerable efforts over the years to improve the PCE of solar cells, The most notable example is the increase in PCE in perovskite solar cells from 3.8% to more than 25% in just a decade [3] This raises the obvious question of whether the PSC can reach the SQ limit. Although state of the art PSCs have already achieved near 1 light absorption and efficient charge collection under short circuit conditions, improving Electroluminescence (EL) quantum efficiency (ELQE) is still an important key to reduce voltage loss and reach SQ limits. Conventional optics show that the out-coupling efficiency of planar elements is limited to $1/4n^2$ (n, refractive index of emitter) and increases to $1/2n^2$ even with rear reflectors, approximately 7.4% (n to 2.6) [4,5] for PSCs. This is already close to the saturation point according to classical optical predictions. It is time to approach through photo-physical methods to find a new method.

3.2. Key index for High efficiency device

3.2.1. Two ways for ELQE enhancement

The fact that the solar cell efficiency exceeds 20% is difficult to explain when photon recycling is excluded. In a situation where the efficiency already exceeds 25%, we repeat absorption and emission of light in the solar cell, and eventually we have to recognize the solar cell as a good LED and think about how to increase the ELQE. For a new path beyond classical limits and toward higher efficiency, it is important to investigate photon recycling (PR) and scattering that can transcend classical limits centered on ELQE and provide a new path toward higher efficiency. (Figure 22) ELQE can also be increased by reducing recombination due to internal defects and reducing photoelectric loss due to field construction. Parastic absorption control is another improvement method. The method is to adjust the thickness of each layer constituting the device or to control the amount of incoming light. The following discussions will prove that the research I have been and will continue to do is aimed at increasing ELQE.
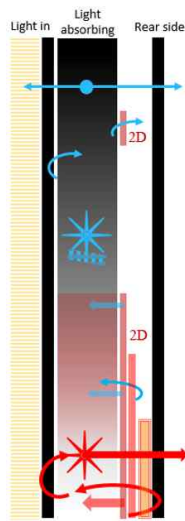
➢ Eleq enhancement

1) Make perovskite as a good illuminant

*increase the absorption ; bandgap control

*increase the emission ; trap passivation

2) Reduce the parasitic absorption

*Optimization of each layer thickness

*Reduce reflected light during incident

Figure 22. Two ways for perovskite's ELQE enhancement

3.2.2. Photon recycling(PR) and scattering in Device

Despite the growing interest in EL in PSCs, there has yet to be an appropriate way to model EL. However, the recent success of high-efficiency PSCs has been impossible without a quantitative understanding of the role of PR and scattering processes. Therefore, we introduce a method that can provide insight to reach the SQ limit when designing a device by setting an optical model that can be generally applied to quantify various optical parameters. At each interface of the PSC stack, the electromagnetic field uses a recently proposed method for LEDs with reabsorption parameters [6,7]. It is assumed that all layers of the device are perfectly smooth and homogeneous. In the case of psc, the scattering effect should be considered for accurate modeling because the active layer is thicker and the particles are larger. We propose an effective scattering coefficient (S0) for quantifying scattering. Assuming an infinite lateral region, the trapped photons are eventually reabsorbed by perovskite (Aact) or parasitic layer (Apara) or scattered at a rate of S0 (Figure 23). At each scattering event, the photon is transformed into a new dipole with arbitrary directions at the same wavelength. Refer to the paper for the correct modeling method.[8,9] Figure 24 shows the outcoupling, Aact, Apara and scattering values of the PSC at each wavelength. PR and scattering recursively generate new

dipoles until no photons remain in the trap mode. Aact is more suitable for short wavelengths, but scattering is more common at long wavelengths where Aact is smaller. Due to these spectral properties, red migration is observed in the external EL in the internal spectrum. Figure 25 shows the relationship between η rad and the calculated external ELQE based on the PR effect [6]. The 1 sun equivalent ELQE 13.7% measured at the PSC is η rad 78%. The ELQE of the direct outcoupling is adrad = 78% to 3.1%, suggesting that PR and scattering can cause ELQE to be approximately 5x higher. At the radiation limit, the maximum ELQE is 34%, and based on the loss, it is still less than 1. PR and scattering improve the ELQE of LED－operated devices, but since Vnr is proportional to the log value, conversion to power output is important to evaluate efficiency in photocell operation. Figure 25 shows the contribution of PR and scattering at each J in the PSC. The ELQE (J) under illumination may be considered to be the same as the ELQE (J+Jph) measured under dark conditions η rad and direct ELQE (except PR and scattering effects) are shown in Figure 26. As the external bias increases, more charge carriers are injected and η rad increases. Scattering reduces Vnr to 14 mV, regardless of η rad, and improves ELQE by 73%. However, the contribution of PR increases as J increases based on improved re－radiation efficiency. More than 78% of photons isolated

from open circuit undergo at least one PR or scattering.

The contribution of scattering to Vnr may not lead to an actual increase in VOC because VOC is the same as Vrad − Vnr and Vrad can also be affected by scattering. Light scattering increases the optical path length of incoming light and improves band edge absorption, reducing apparent bandgap and Vrad [9]. Vnr and Vrad keep VOC unchanged [10], which means that the scattering process improves the photocurrent without voltage loss, leading to a trade off between Jph and VOC. In short, it is reasonable to think that the decrease in Vnr due to scattering will continue to cause a net increase in PCE without changing Vrad or photocurrent.
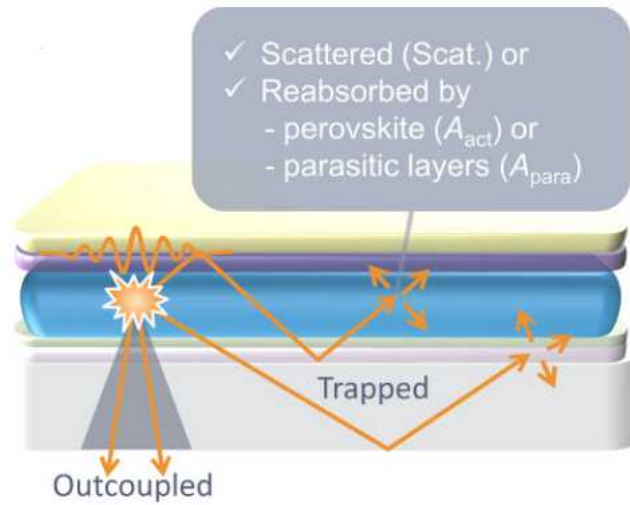
Figure 23. Schematic of light emission and trapped modes in PSCs.
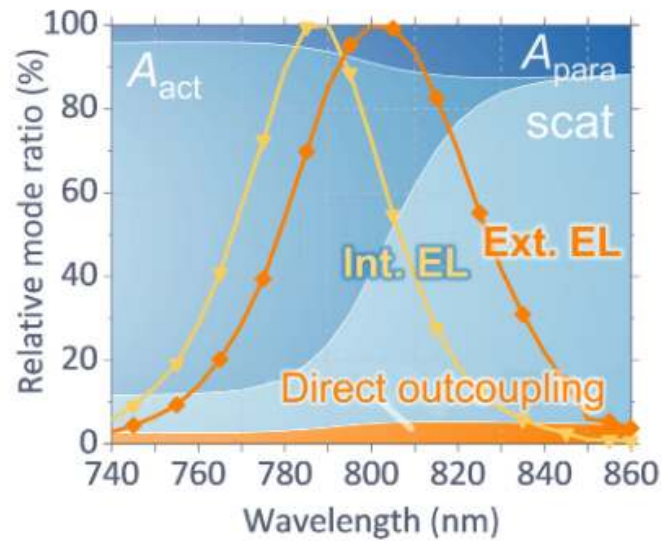
Figure 24. Calculated fractions of outcoupling, scat, Aact, and Apara at each wavelength (background). The external EL spectrum is obtained by considering PR and scattering effects for an η_{rad} of 78%.
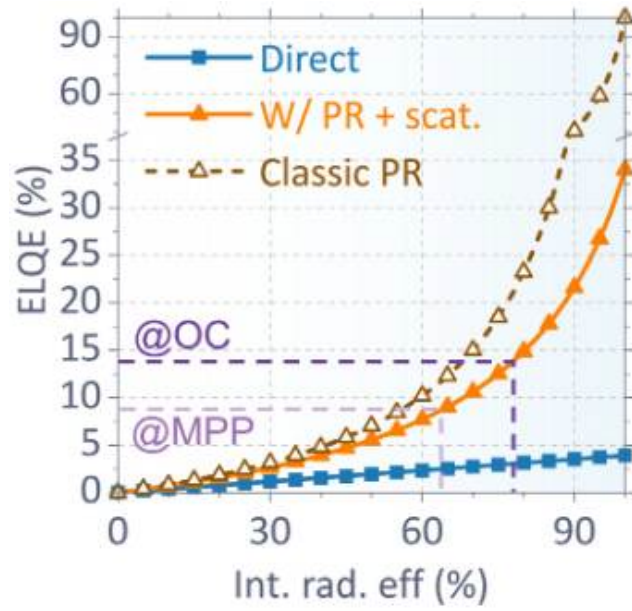
Figure 25. Calculated ELQEs of a full device as a function of ηrad, including and excluding PR and scattering effects. The brown dashed line is derived from a classical calculation ignoring Apara and scattering.
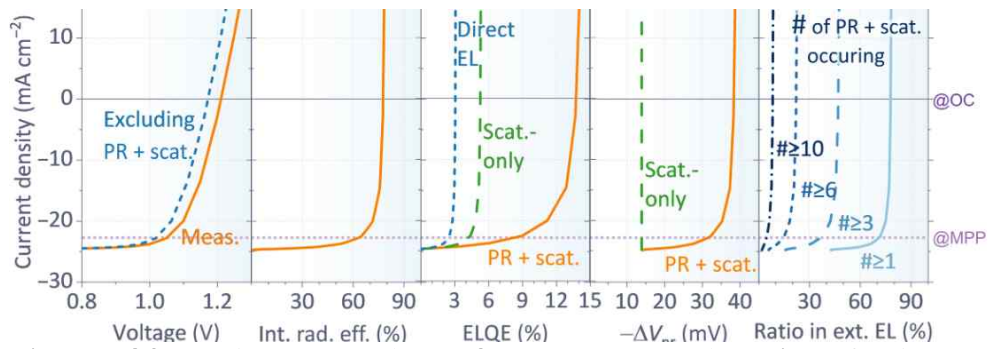
Figure 26. Voltage, ηrad, ELQE, $-\Delta$Vnr, and ratio of photons undergoing given number of recursive PR and scattering events in external EL as functions of J for our PSC. MPP, maximum power point.

3.3. High efficiency Photovoltaic device

3.3.1. Device fabrication

Synthesis of (BA)2PbI4 crystal powder.

A mixed solution (16 ml) of HI solution and an H3PO2 solution (2 ml) were prepared together in a 200 ml glass volumetric flask. PbO powder (2,232mg, 10mmol) was heated and dissolved while stirring, and 993 μl of butylamine (10mmol) was added to the solution and the stirring was stopped. The temperature is slowly lowered by leaving the solution at room temperature, forming orange crystals. Separation of crystals by suction filtration; It is completely dried in the vacuum chamber.

Perovskite film coating process

Clean a 2.5 cm x 2.5 cm glass substrate coated with tin−doped indium oxide (ITO) with deionized water, acetone, ethanol and isopropyl alcohol for 15 minutes, respectively. The substrate was ozone−treated in ultraviolet light for 15 minutes, and the precursor was hooked into a DMF/DMSO (8:1 v/v) mixed solvent and spin−coated on the substrate at 5,000 rpm. During the 20−second interval, diethyl ether was quickly poured onto the substrate in 10 seconds. The yellow film was quickly moved to a hot plate and heat treated at

100 °C for 5 minutes. The 3D perovskite film is manufactured differently only in the precursor of the solution. However, it is formed on a 50 nm SnO_2 substrate grown by chemical bath deposition on an FTO substrate, not an ITO substrate.

SIG process.

Hot press method was used to fabricate 3D/SIG-2D film. The pre-produced (BA) 2PbI4 thin film was placed on the 3D thin film and pressed at a desired temperature (30 °C, 45 °C, 60 °C) for 10 minutes at 60MPa. To analyze growth at various pressures of SIG treated 2D thin films, the pressure (20 MPa, 40 MPa or 60 MPa)

Manufacture of hole transport layer and counter electrode

A Spiro-OMeTAD solution in which 23 μl of bis(trifluoromethanesulfonyl)imide (Li-TFSI) (540 mgml^{-1}) of acetonitrile, 375 mgml^{-1}) and 39 μl of 4-tert-butylpyridine were added was added. 2,000 r.p.m. for 30 seconds on a substrate coated with FTO/SnO_2/3D/(SIG-2D). An undoped P3HT solution (mixed solvent of chlorobenzene: diphenyl ether = 10 mgml^{-1} in 97:3 v/v) was used for the humidity stability test, while a PTAA solution (12 mgml^{-1} in toluene) was 6 μl Li-TFSI (340 mgml^{-1} of acetonitrile) and 6 μl of 4-tert-butylpyridine were used in attenuation heat tests.

Finally, the gold counter electrode was deposited by thermal evaporation. The active area of the counter electrode was fixed at 0.16 cm^2.

3.3.2. SIG-2D:3D based High efficiency Photovoltaic device

Figure 27 shows a summary of the parameters for device performance for SIG60 devices with current density-voltage (J-V) curves and FTO/SnO2/perovskite/spiro-OMeTAD/Au structures. open circuit voltage (VOC) is significantly improved over conventional control devices, with PCE from 22.39% to 24.59%, short circuit current (JSC) 24.70 mAcm^{-2}, open circuit voltage (VOC) 1.185 V, Fill factor (FF) 83.90%). It also has negligible J-V hysteresis and stable power output at maximum power points.(Figure 27 and Figure 28) This was shown by increasing this thickness from 0 nm (control group) to 40 nm (SIG30) to 80 nm (SIG60), focusing on the formation of the depletion layer in the two-dimensional perovskite, as discussed earlier. In fact, the VOC increased from 1.098 V to 1.117 V

Finally, it increased to 1.185 V, resulting in a gradual increase in PCE (Table 4). The JSC values were almost similar regardless of thickness. The fill factor value is slightly improved from 82.95% to 83.90%. It is very encouraging that the fill factor has improved despite the increase in the series resistance from 5.39 to 6.60, presumably due to the low conductivity of 2D perovskite (Figure 29). This means that the positive effects of the surface passivation and rear fields of the 2D layer outweigh the negative effects of the series

6 3

resistance to the fill factor. The statistical data in Figure 30 also show that improvements in VOC are reproducible and important for high PCEs in SIG60 devices. The TRPL results in Figure 15 indicate that in addition to the reduction of surface recombination, other factors are involved. Band bending in 2D/3D heterogeneous junctions in Figure 31 can have a positive effect on VOC in the improvement of VOC. We ran a Mott−Schottky plot analysis to confirm the Vbi change in the SIG device. Reliable Mott−Schottky plot analysis methods for internal field measurements are discussed again in the following. An increase in the internal field is associated with an increase in thickness. Vbi increases with increasing 2D thickness despite similar photoluminescent carrier life. This result confirms once again that the Vbi obtained using the 2D layer could be designed in 2D. As a result, the SIG−$(BA)_2PbI_4$ layer maintained its unique properties while being stacked to a thickness of several tens of nanometers, enabling improved device performance.

	J_{SC} (mA cm^{-2})	V_{OC} (%)	FF (%)	PCE (%)
F	24.61	1.093	82.76	22.26
R	24.59	1.102	83.14	22.52
A	24.60	1.098	82.95	22.39
F	24.71	1.187	83.67	24.54
R	24.67	1.183	84.22	24.63
A	24.70	1.185	83.90	24.59
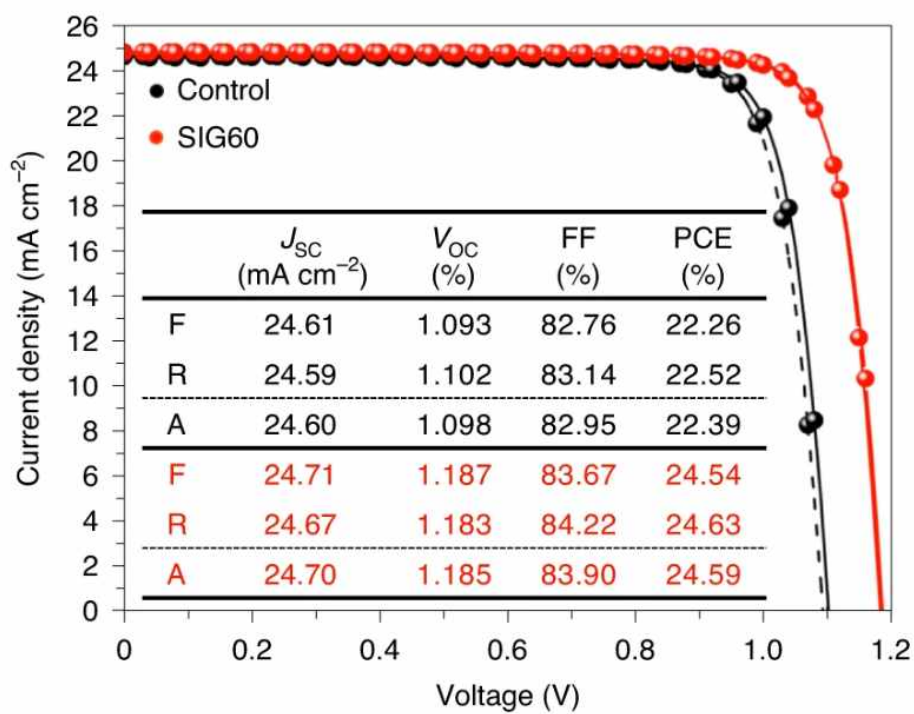
Figure 27. A comparison of the photovoltaic performances of the control (FTO/SnO₂/3D/spiro−OMeTAD/Au) and SIG60 (FTO/SnO₂/3D∶(SIG−2D)/spiro−OMeTAD/Au) devices. Solid lines and dashed lines indicate the reverse and forward scans, respectively.
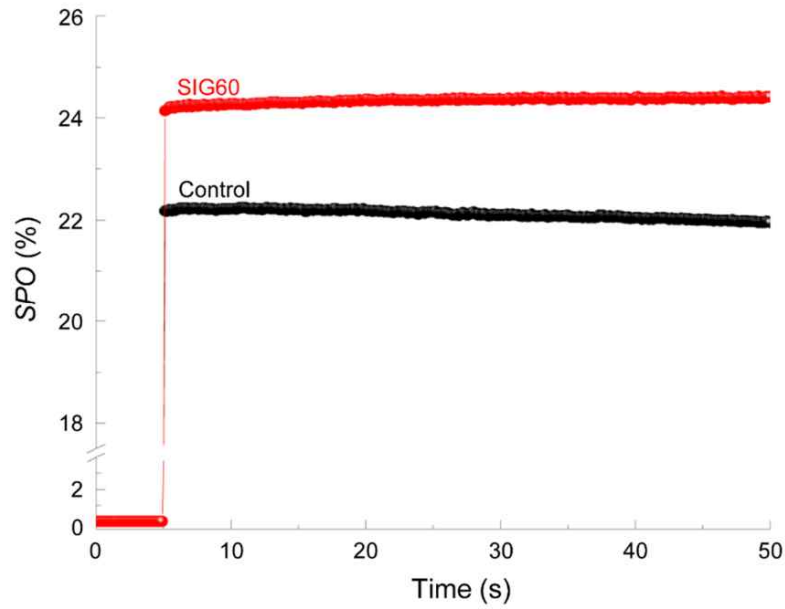
Figure 28. Stabilized power output (SPO) of the control and SIG60 devices. Unencapsulated control and SIG60 devices were measured for 50 s at a fixed voltage under simulated AM 1.5G (100 mW/cm^2) in air. The fixed voltage was set to the maximum power point identified from the J−V curve (control: 0.98 V, SIG: 1.01 V).

Device type		J_{SC} (mA/cm^2)	V_{OC} (V)	FF (%)	η (%)
Control	Average	24.56 ± 0.13	1.094 ± 0.005	81.73 ± 0.73	21.95 ± 0.24
	Champion	24.60	1.098	82.95	22.39
SIG30	Average	24.61 ± 0.07	1.118 ± 0.002	81.96 ± 0.39	22.55 ± 0.11
	Champion	24.75	1.117	82.30	22.75
SIG45	Average	24.57 ± 0.17	1.140 ± 0.010	81.57 ± 2.00	22.85 ± 0.63
	Champion	24.68	1.145	84.09	23.76
SIG60	Average	24.64 ± 0.12	1.169 ± 0.011	82.11 ± 1.07	23.67 ± 0.41
	Champion	24.70	1.185	83.90	24.59

Table 4. Summary of the photovoltaic parameters of devices according according to the processing temperature. All parameters were obtained from current density−voltage (JV) curves measured under 1 sun illumination. Average parameters are displayed as the average value and standard deviation. For each device type, the average parameters were obtained from the arithmetic mean of eight devices.
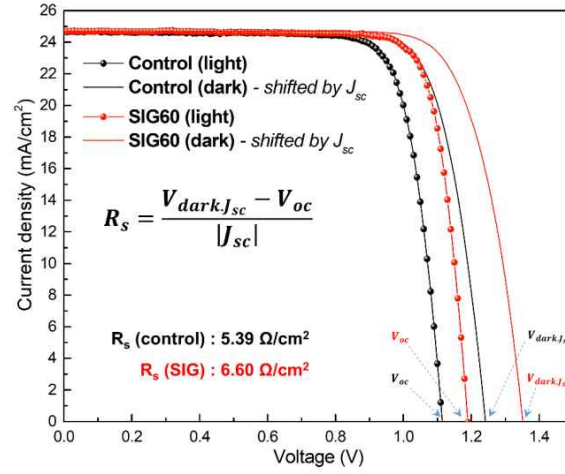
Figure 29. Series resistance of control and SIG devices. Series resistances were calculated from the J−V curves. Series resistance of the control and SIG devices measured under 1 sun illumination and in the dark.
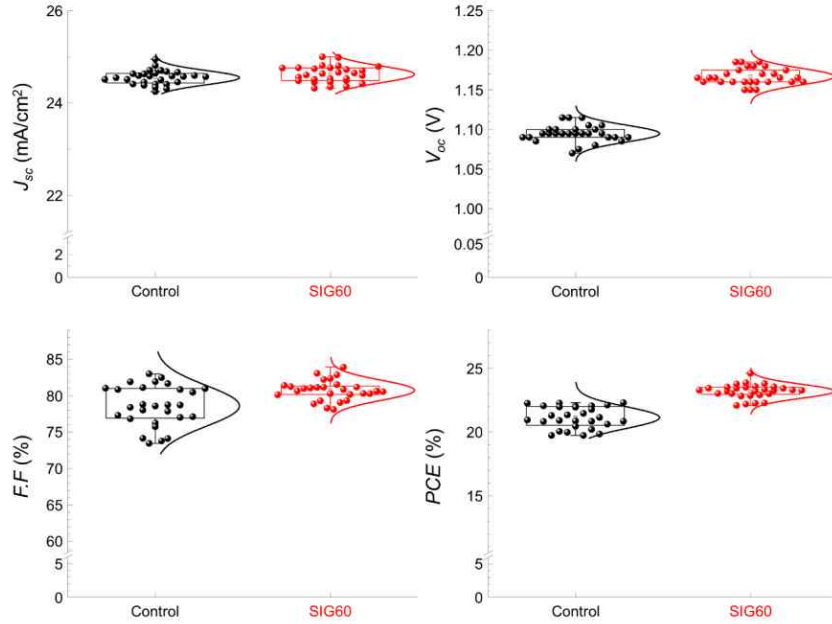
Figure 30. Statistical data of the short−circuit current density (JSC), opencircuit voltage (VOC), fill factor (FF) and power conversion efficiency (PCE) for both control and SIG60 devices. All parameters were obtained from 28 cells for both control and SIG60 devices. Each box represents the first quartile to third quartile of data, and the upper and lower points of the error bars show the minimum and maximum values. All performances were detected using a shadow mask of 0.094 cm^2 at room temperature in air.
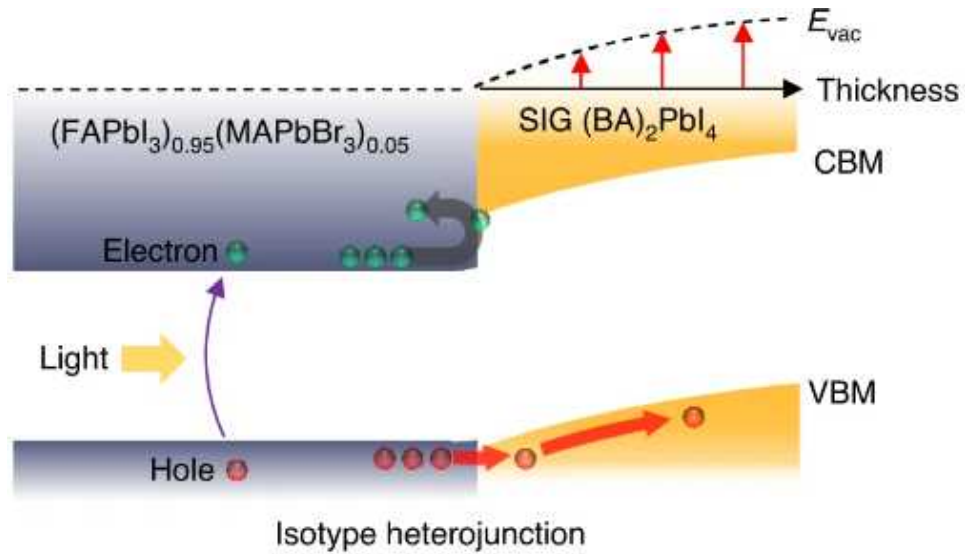
Figure 31. Built-in potential change induced by 2D/3D heterojunction formation. The grey and red thick arrows indicate flow of photogenerated holes and photogenerated electrons, respectively, whereas the purple arrow indicates excitation of electron caused by light. The black narrow line represents the thickness change of the 2D perovskite and the orange narrow lines are the vacuum level change caused by it.

3.3.3. Analysis of device field enhancemnet

In Table 2 and Figure 16, we have already discussed that there may be an increase in life time due to surface passivation. However, the passivation due to the increase in life time is not sufficient to explain all the increase in the field of the preceding device. In particular, since the increase in life time does not increase proportionally depending on the thickness, this means that it does not depend on temperature. This result is very peculiar, because even though the VOC, which is very related to the field of the device, increased, the life time did not match the trend. In fact, the elimination of surface defects by 2D perovskite is usually represented as non-radiative recombination, but it is not properly mentioned what kind of defect it is. In fact, it is difficult to analyze and confirm the state of the product itself with a solution process with low reproducibility. However, since it reacts with PbI_2 or $ApbI_3$, we can guess that it probably does not produce halide defect dependent results. However, based on some hints, we can think about what defects are eliminated in the SIG-treated perovskite surface. Defects present on the surface of perovskite are mainly uncoordinated Pb, halide vacancy, and organic vacancy, which have the effect of applying strain to the surface. (Figure 32)[11] Depending on the degree of strain relief, the bandgap of the material may change or the lifetime of the carrier may

6 9

be affected. In fact, some organic spacers, including PEA (Phenylethylamine), show strain relief in the lattice due to A-site alloying. [12] In the case of BA (Butylammonium), which is very similar to this organic spacer, it is assumed that a similar reaction occurred as some BA was mixed into the A site vacancy because it forms an undamaged SIG bond. If the reaction occurs above a certain level, the strain changes the bulk characteristics, and changes such as bandgap may occur. However, in the case of $(BA)_2PbI_4$ used in Figure 33, such a change does not appear. Therefore, it is thought that the surface passivation by the above and SIG was targeted by a cation defect that relieves strain that is very limited to the surface.

However, as we mentioned earlier, the increase in life time did not explain the increase in VOC, and specifically, it did not fully explain the increasing tendency of the internal field, which increases dependently on the 2D thickness. This is closely related to the fact that the thickness of the material layer having a low intrinsic carrier concentration in the p-type heterojunction determines the degree of the field enhancement. [13] To actually measure these changes, I looked at the change in the internal field of the device according to the 2D thickness.

Mott-Schottky(MS) is simple by checking the formation of fields in the dielectric section, but it is very useful for predicting the fields formed within the element if you have precise measurement conditions. A perovskite solar cells based MS plot analysis is already reported. [14] To identify a reliable built-in potential, the MS plot and capacitance-voltage curve of the PSC must first distinguish three regions: the electrode polarization capacitance dominance region (Cs), the depletion layer capacitance dominance region (Cdl), and the geometric capacitance dominance region (Cg). To accurately measure MS plots, consider the following steps:

(Step 1) Identification within the spectrum of capacitance in the frequency range, (Step 2) Appropriate measurement frequency within the central stabilizer of the capacitance spectrum, (Step 3) Identification of voltage regions governed by the depletion layer capacitance Cdl, (Step 4) Verification of sensitivity of MS analysis to scan direction and speed. Following the above steps, MS plot measurements were divided into four steps to obtain appropriate information about the newly formed embedded potential in 2D/3D junctions.

Step 1) Identification within the capacitance spectrum of the frequency range. Capacitance was measured as a function of

frequencies from 10^1 to 10^6 Hz to identify dielectric polarization regions, stable regions of the capacitance spectrum, containing additional contributions of the depletion layer capacitance Cdl. We find that sections below approximately 5 kHz are electrode polarization regions where capacitance increases exponentially when several electrical biases are applied, as shown in Figure 34a. In contrast, the tendency of capacitance with frequency changes to a plateau at frequencies above 5 kHz, meaning that the capacitance mechanism depends much more strongly on dielectric polarization.In the capacitance spectrum, we can identify two regions: electrode polarization and dielectric polarization for PSC.

Step 2) Select the appropriate measurement frequency within the center stabilizer of the capacitance spectrum. In Figure 34a, the appropriate frequency domain can be selected at 5×10^3 Hz to 10^6 Hz for the dielectric polarization region to measure the built−in potential of the PSC affected by the depletion layer. However, the contribution of the depletion layer capacitance Cdl at all frequencies does not appear in the MS plot. Therefore, the appropriate measurement frequency was selected in the next step.

Step 3) Identification of the voltage region dominated by the

depletion layer capacitance (Cdl) Capacitance-voltage measurement was carried out in the dielectric polarization region to confirm the contribution of the depletion layer capacitance (Cdl). All measurements were made forward at 2 mV/s. It was determined that the contribution of Cdl is clearly shown in the MS plot at 10 kHz in Figure 34b, while the contribution of Cdl is not shown at 100 kHz in Figure 34c. As shown in Figure 31b, the correct MS analysis requires the separation of three voltage zones, allowing you to select the appropriate frequency of 10 kHz.

Step 4) Verification of MS analysis sensitivity for scan direction and speed. We investigated the behavior of MS plots that changed the scan direction to determine the measurement conditions of the scan direction and speed for the last acquired MS plots. Speed at a fixed frequency of 10 kHz. Figure 34d shows MS plots obtained from different scan directions and speeds at 10 kHz. The slow scan rate (2 mV/s) shows negligible hysteresis, while the fast scan rate (12 mV/s) shows obvious hysteresis in the MS plot. Therefore, we have confirmed that the measurement conditions of scan direction (forward direction), scan speed (2 mV/s), and frequency (10 kHz) are suitable for MS plot analysis for PSC. The steps above the Mott-Schottky plot for the control and SIG units obtained a reliable MS plot

for the control and SIG units under the selected measurement conditions (2 mV/s, forward scanning, 10 kHz). The plots are shown in Figure 35. All MS plots clearly show the Cdl area. Therefore, The built−in potential (Vbi) for all devices can be obtained by linear fitting derived from Equation below.

$$C_{dl} = \sqrt{\frac{q\varepsilon\varepsilon_0 N}{2(V_{bi}-V)}}$$

where q is the elementary charge, $\varepsilon 0$ is the vacuum permittivity, ε is the relative dielectric constant of the perovskite material, N is the carrier density, and Vbi is the built−in potential. The obtained Vbi values along with VOC values for devices are summarized in Table 5.
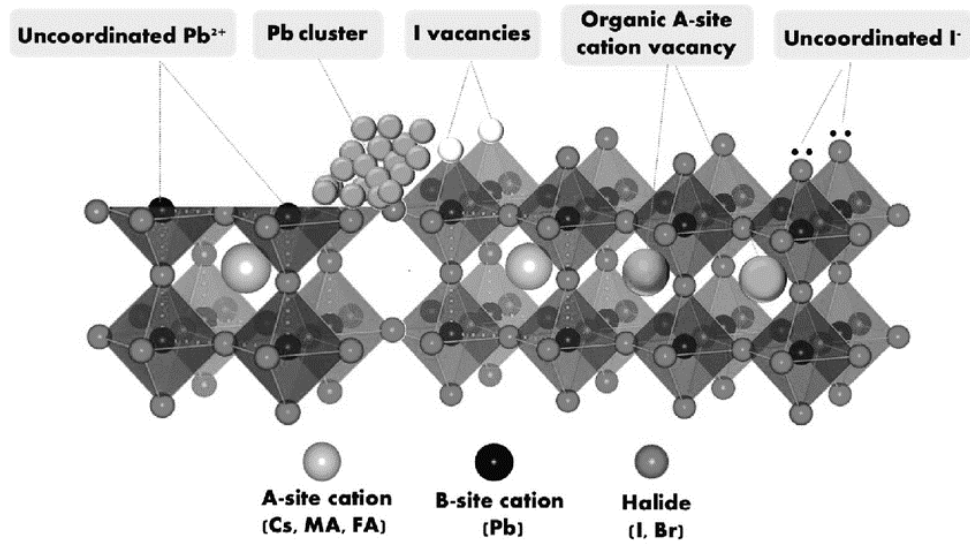
Figure. 32. Different types of surface defect of perovskite. This image is adapted. [11]
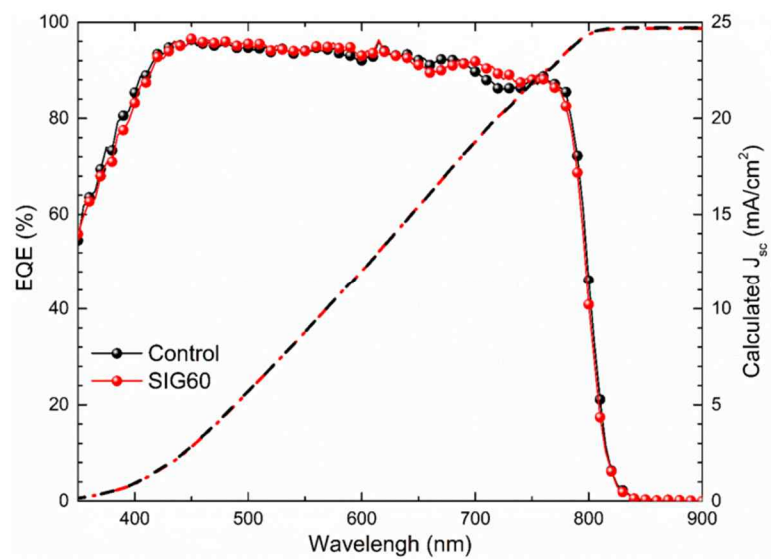
Figure 33. External quantum efficiency and calculated short circuit current density of control and SIG60 devices. EQE spectrum as a function of monochromatic wavelength for the control and SIG60 devices. This image is adapted. [13]
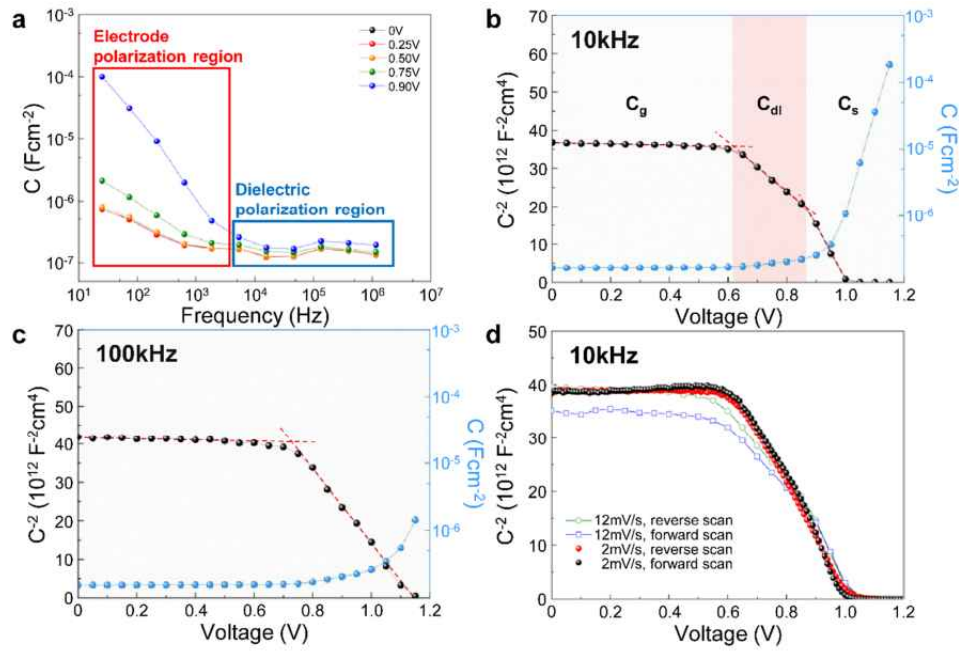
Figure 34. Capacitance-frequency spectrum, capacitance-voltage curve, and Mott-Schottky plot. a. Capacitance-frequency spectrum of our control device (FTO/SnO2/3D/Spiro-OMeTAD/Au) at a DC forward bias in the dark. b-c. MS plot and capacitance-voltage curve of the control device at 10 kHz and 100 kHz in the dielectric polarization region. The red dashed line is a guideline to show a distinct capacitance mechanism region in each MS plot. Cg, Cdl, and Cs indicate geometrical capacitance, depletion layer capacitance, and electrode polarization capacitance, respectively. d. Scan rate and direction effect on the MS plot at 10 kHz.
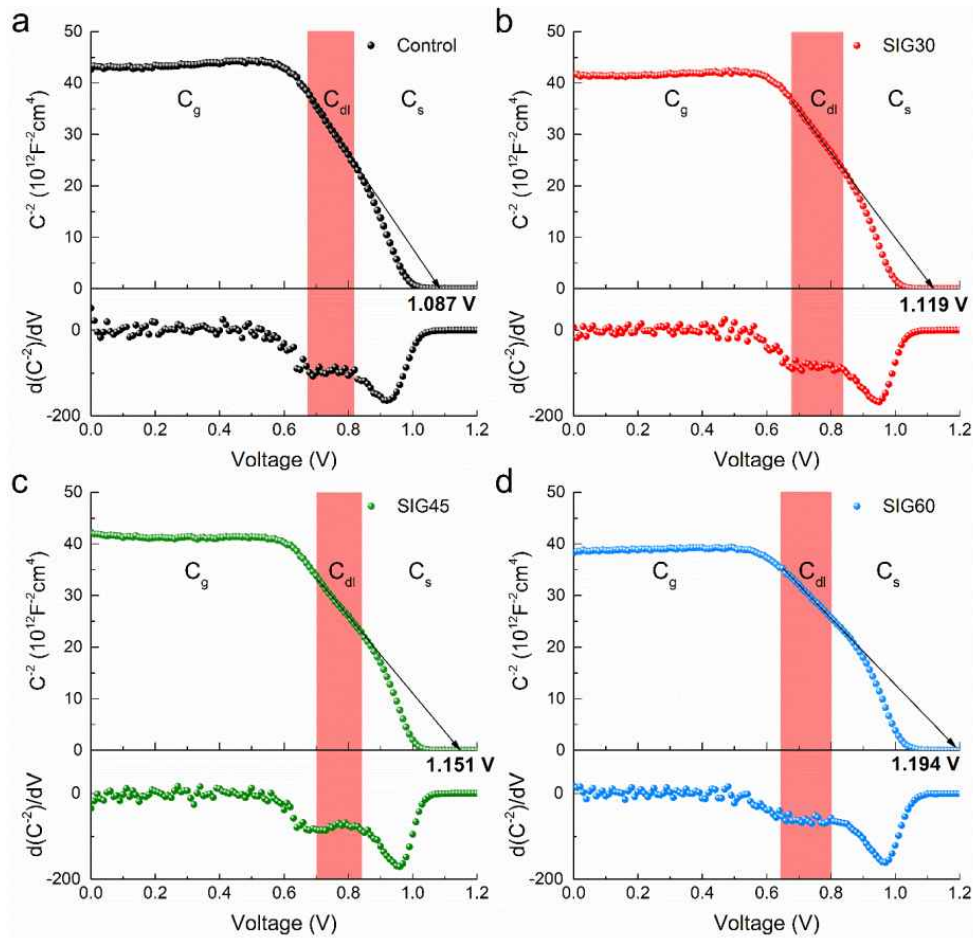
Figure 35. Mott−Schottky plot of control and SIG devices. The MS plot measurement conditions were determined to be a 10 kHz frequency, a forward scan direction, and a 2 mV/s scan rate based on Figure 34. To extract the built−in potential from each MS plot, a linear function was fitted using a derivative of C^{-2}

Condition	2D thickness (nm)	First-order lifetime (μs)	V_{bi} of MS plot (mV)		V_{OC} of each device (mV)		V_{bi} from Eq. (S5) (mV) $N_{2D} = 1.67 \times 10^{16} cm^{-3}$
			V_{bi}	ΔV_{bi}	V_{oc}	ΔV_{oc}	V_{bi}
Control		0.20	1087	-	1098	-	-
SIG30	42.30 ±1.18	1.05	1119	**32**	1117	**19**	**28.48 ± 1.59**
SIG45	60.70 ±1.09	1.00	1151	**64**	1145	47	**58.62 ± 2.11**
SIG60	83.45 ±1.45	1.11	1194	**107**	1185	87	**110.80 ± 3.84**

Table 5. Change in the built−in potential and open−circuit voltage in SIG devices.

3.4. Optical approach

3.4.1. Anti-reflective film

Note: This chapter is reproduced from the work I co-authored with Seongmin Kang published in Advanced Energy Materials, 12 (33), 2201520.

The above-mentioned method of increasing ELQE is the same as how good it is as an LED. This is related to how well light can form and come back out. For this reason, light entering the device is often overlooked, which is about 5% of light in actual calculations, but it is a value that cannot be ignored when considering the photoelectron mutation effect in the effect of increasing absorption for each wavelength. Therefore, Professor Kang Seongmin's team at Chungnam National University devised a method to achieve the highest efficiency and commercialization of perovskite solar cells (PSCs) by improving the light transimition efficiency (LTE) of sticker AR (anti-reflection) films (Figure 36). Previously, materials used in AR films had high reflectivity and high rigidity due to limitations in physical properties, making it difficult to apply them to high-efficiency flexible devices. Therefore, we propose a method to increase the total absorption of light by devising a sticker-type ultra-thin perfluoropolymer PFPE AR film (SUPA) made of PFPE (n = 1.34) manufactured through a designed two-stage peeling

propagation method.[15] In fact, the proposed SUPA presents a high LTE (98.3%) value, and the film thickness is also very thin, about 20 μm. It represents the highest level of actual AR performance reported. Based on the high EQE increase, the JSC value of 26.63 mAcm^{-2} was secured (Figure 37). It is stably driven even under light exposure 168h and wet heat conditions 1000h. It maintains an initial transmittance of 97.5% or more, and the SUPA-applied device is stably driven even on a 2mm radius base of the bending test.
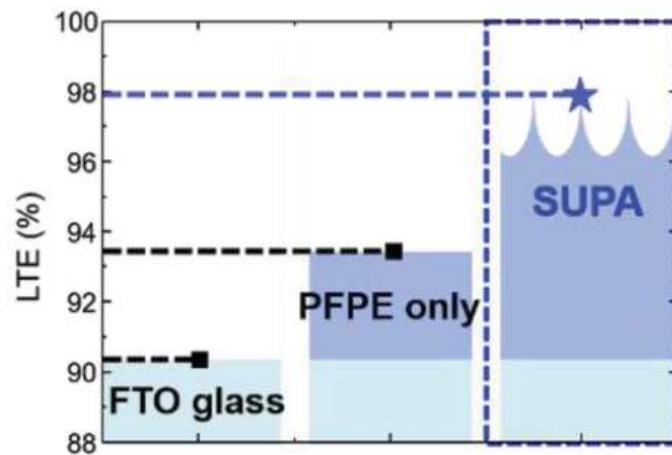
Figure 36. Calculated Improvemnet of LTE of fluorine-doped tin oxide (FTO) glass and with attaching PFPE only surface and SUPA. This figure is adopted from reference[15]
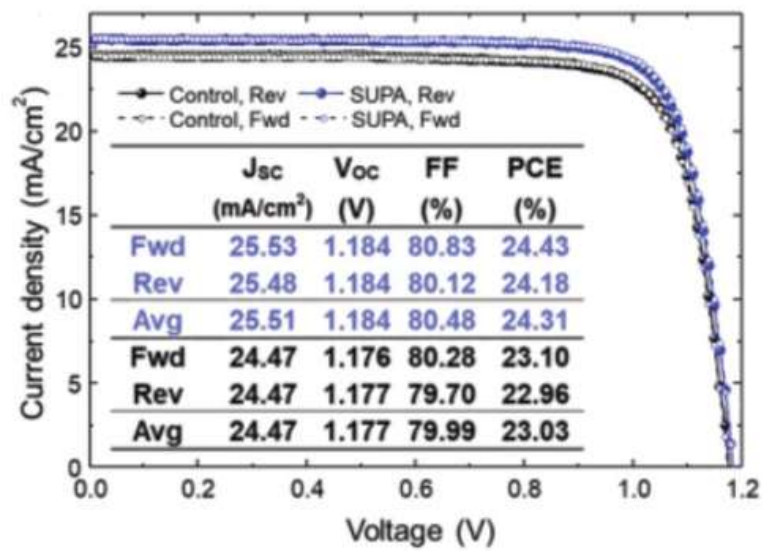

Figure 37. Performance of rigid PSC with SUPA and mechanical durability of SUPA. This figure is adopted from reference[15]

3.4.2. Vertical charge transport measuring

In order to improve the new 2D perovskite usage method, it is also important to understand the parameters for each of 3D and 2D perovskite. In particular, in order to understand the effect of tube conversion, the understanding of diffusivity should be based on. Understanding the rapid diffusion of charge carriers is the most important factor in efficient charge collection in perovskite solar cells. There is a discrepancy between the previously widely used low charge diffusion coefficient of perovskite measured through a lateral transient photoluminescence microscope and the near-one charge collection efficiency achieved in real solar cells. Clearly, there is a problem with the measurement method, which makes it difficult to devise a proper charge collection structure. Therefore, I and Dr. cho changsoon of Cambridge University characterized the out-of-plane diffusion of carriers and tried to reveal the hidden microscopic dynamics of halide perovskites through four-dimensional (4D – x, y, z, t) tracking of charge carriers (Figure 38).[16] With this approach using confocal microscopy, we find strong local heterogeneity of vertical charge diffusion in 3D perovskite films. And this happens because there is a difference in the degree of diffusion between the particles inside. We also visualized that charge carriers are

transported efficiently via direct intraparticle routes or indirect bypasses through nearby regions. The anisotropy and heterogeneity of charge carrier diffusion in perovskites demonstrate the high performance shown in real−world devices. Solar cells with micrometer−thick perovskites can simultaneously analyze long optical path lengths and efficient charge collection. We also measured the diffusivity in the inplane and out of plane directions of 2D perovskite using a method that can measure this anisotropy at the same time, and found that the difference was more than 10 times (Figure 39).
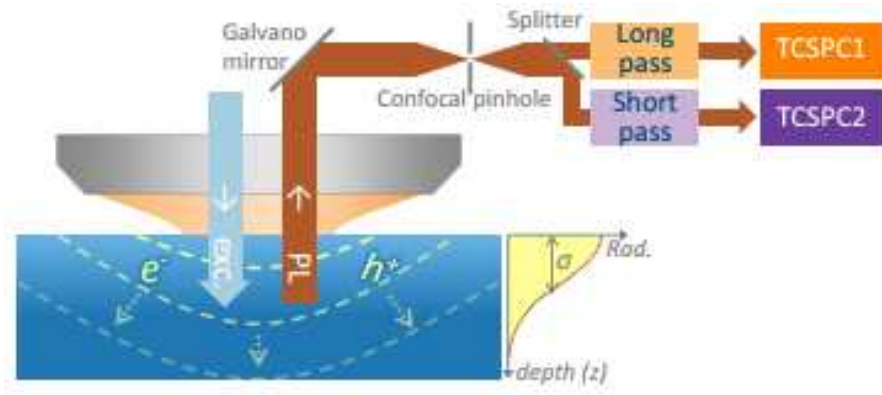
Figure 38. Vertical charge transport mesuring This figure is adopted from reference[16]
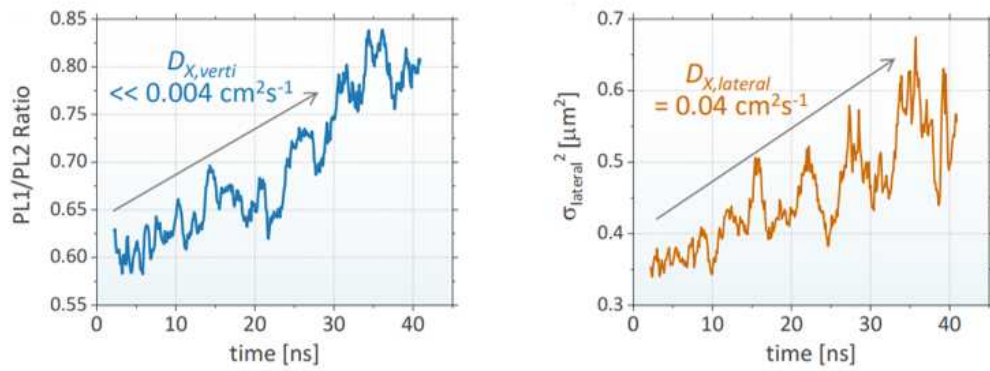
Figure 39. The diffusivity of 2D perovskite in the inplane and out of plane directions. This figure is adopted from reference[16]

3.5. Conclusion

The development of PSC is almost at a limit from the standpoint of Shockley－Queisser (SQ) theory. In order to overcome this, it is necessary to understand the existence of PR and the defects affecting the inner field. In other words, a high ELQE will be an accurate research direction to make good devices. The SIG process has various approaches to this. Better elqe can be made by adjusting the thickness of each layer, or by strengthening the internal field and passing the defect. In addition, controlling the parastic loss can reduce the loss in the process of light moving inside and outside the device, and to that end, I devised a SUPA film using PFPE with a low reflective index. For high－efficiency devices in the future, it should be a direction for making elqe high devices.

3.6. References

[1] Shockley, W., & Queisser, H. J. (1961). Detailed balance limit of efficiency of p-n junction solar cells. Journal of applied physics, 32(3), 510-519.

[2] Miller, O. D., Yablonovitch, E., & Kurtz, S. R. (2012). Strong internal and external luminescence as solar cells approach the Shockley-Queisser limit. IEEE Journal of Photovoltaics, 2(3), 303-311.

[3] Yoo, J. J., Seo, G., Chua, M. R., Park, T. G., Lu, Y., Rotermund, F., ... & Seo, J. (2021). Efficient perovskite solar cells via improved carrier management. Nature, 590(7847), 587-593.

[4] Greenham, N. C., Friend, R. H., & Bradley, D. D. (1994). Angular dependence of the emission from a conjugated polymer light-emitting diode: implications for efficiency calculations. Advanced Materials, 6(6), 491-494.

[5] Yablonovitch, E. (1982). Statistical ray optics. JOSA, 72(7), 899-907.

[6] Cho, C., Zhao, B., Tainter, G. D., Lee, J. Y., Friend, R. H., Di, D., ... & Greenham, N. C. (2020). The role of photon recycling in perovskite light-emitting diodes. Nature communications, 11(1), 1-8.

[7] Sridharan, A., Noel, N. K., Rand, B. P., & Ke·na-Cohen, S.

(2021). Role of photon recycling and band filling in halide perovskite photoluminescence under focussed excitation conditions. The Journal of Physical Chemistry C, 125(4), 2240-2249.

[8] Cho, C., & Greenham, N. C. (2021). Computational Study of Dipole Radiation in Re-Absorbing Perovskite Semiconductors for Optoelectronics. Advanced Science, 8(4), 2003559.

[9] Polman, A., & Atwater, H. A. (2012). Photonic design principles for ultrahigh-efficiency photovoltaics. Nature materials, 11(3), 174-177.

[10] Brenes, R., Laitz, M., Jean, J., deQuilettes, D. W., & Bulović, V. (2019). Benefit from photon recycling at the maximum-power point of state-of-the-art perovskite solar cells. Physical Review Applied, 12(1), 014017.

[11] Lu, H., Krishna, A., Zakeeruddin, S. M., Grätzel, M., & Hagfeldt, A. (2020). Compositional and interface engineering of organic-inorganic lead halide perovskite solar cells. Iscience, 23(8), 101359.

[12] Wang, H., Zhu, C., Liu, L., Ma, S., Liu, P., Wu, J., ... & Chen, Q. (2019). Interfacial residual stress relaxation in perovskite solar cells with improved stability. Advanced Materials, 31(48), 1904408.

[13] Jang, Y. W., Lee, S., Yeom, K. M., Jeong, K., Choi, K., Choi, M., & Noh, J. H. (2021). Intact 2D/3D halide junction perovskite solar cells via solid-phase in-plane growth. Nature Energy, 6(1), 63-71.

[14] Almora, O., Aranda, C., Mas-Marzá, E., & Garcia-Belmonte, G. (2016). On Mott-Schottky analysis interpretation of capacitance measurements in organometal perovskite solar cells. Applied Physics Letters, 109(17), 173903.

[15] Choi, J. S., Jang, Y. W., Kim, U., Choi, M., & Kang, S. M. (2022). Optically and Mechanically Engineered Anti-Reflective Film for Highly Efficient Rigid and Flexible Perovskite Solar Cells. Advanced Energy Materials, 12(33), 2201520.

[16] Cho, C., Feldmann, S., Yeom, K. M., Jang, Y. W., Kahmann, S., Huang, J. Y., ... & Greenham, N. C. (2022). Efficient vertical charge transport in polycrystalline halide perovskites revealed by four-dimensional tracking of charge carriers. Nature Materials, 1-8.

Chapter 4. Commercialization issue

4.1. Introduction

There are various factors in the decomposition of perovskite and other PSC components. The stability problems can be divided into stability problems inherent in the molecular and crystallographic structures of perovskite and stability problems caused by other components or external factors of PSC. However, although most of them can be solved by encapsulation, this causes a rapid increase in process prices, so efforts are needed to remove internal factors and keep the device stable. In particular, ensuring sufficient stability has become more important than ever, as the efficiency of PSCs has already exceeded 25% in laboratory scale experiments.

For commercialization, a technology that can secure stability and reliability is needed. In addition, simultaneous development of large area and high efficiency devices is required. In this chapter, we will discuss attempts to achieve large-area devices with high efficiency while preventing degradation.

4.2. Stability issue

4.2.1. Understanding of low stability

Perovskite has been found to have satisfactory intrinsic stability compared to its counterpart. However, perovskites used in the device are affected by external factors such as heat, moisture, light, and interfacial materials. [1] Because perovskite and PSCs are unstable for these factors, it is very important to understand the deterioration of PSCs due to these external factors and to take appropriate measures to mitigate the problem.

Reversible and irreversible decomposition of light harvester perovskites was discussed in the previous section. The PSC also requires other components. They can also deteriorate when heated at slightly higher temperatures. Spiro-OMeTAD can crystallize at 100 ℃, reducing solar cell efficiency. The additives used with Spiro-OMeTAD evaporate even at much lower temperatures of 85 ℃. [2, 3] The encounter with moisture is more deadly. Once perovskite is contacted by moisture, a reaction by irreversible water occurs and produces CH_3NH_3I and PbI_2. [4] The effects of water are already known in many studies. [5, 6] To address this, research is also being conducted on 2D perovskite, which lowers the dimension of crystal

structure, but there is a trade-off of efficiency and stability, and a

separated layer, 2D:3D structure, has been adopted to prevent it.

4.2.2. Stable device based on 2D perovskite

It was expected that the SIG device that can take the stability of 2D perovskite and the high light conversion efficiency of 3D perovskite at the same time will have high resistance to the environment. The reason is that the organice spacer prevents moisture penetration and suppresses the leakage of ions. [7] The stability of the 2D perovskite surface in the pure (n=1) state is superior to that of the 3D perovskite film in which volatile cations are distributed near the surface. [8] As a control device to compare the reactivity with water (Experiments with FTO/SnO2/3D) structures and SIG films (FTO/SnO$_2$/3D:SIG-2D) once again confirm the superior stability. The stability of the thin film, estimated by measuring the UV absorption after exposure to 85% relative humidity and room temperature, shows that the SIG film maintained its initial state. (Figure 40) Absorbance even after 1,000 h in contrast to the control film. The humidity stability test of the device was performed with undoped P3HT to exclude and evaluate the moisture and heat instability of spiro-ometad mentioned above (Figure 41). Non-encapsulated controls (FTO/SnO$_2$/3D/P$_3$HT/Au) degraded 41.4% after 400 hours, while unencapsulated SIG devices (FTO/SnO2/3D:SIG-2D/P3HT/Au) had 1,083 After h, it shows only 2.7% (average) degradation compared to the initial PCE. It was

9 2

observed that unencapsulated SIG devices stored under atmospheric conditions at room temperature in the dark retained their initial PCE even after 7,000 hours. Figure 42 shows the results of the decay heat test of the SIG device using encapsulated PTAA at a relative humidity of 85℃/85% or less. The most stably encapsulated SIG device maintained 95% of the initial efficiency of 21.34% even after 1,056 hours in this experiment.

The topology grown by the SIG process provides excellent operational stability as a perfect 2D/3D heterojunction, making it possible to secure thermal stability.

As important as the thermal environment, how stable it operates in the light irradiation environment. Figure 43 is a graph of SPO (stable power output), which shows repeated measurements of device efficiency in a continuous light exposure environment. It maintains more than 24% efficiency under one sun illumination condition for more than 1600 hours. This is very encouraging in terms of commercialization of the device. More than 21% of common devices include 2D perovskite-based processes. As mentioned repeatedly, this process forms materials in an unstable quasi-2D state, and the efficiency of devices containing these materials does not remain stable. In fact, in most devices, an initial drop exists within 100 hours. However, the SIG-2D device does not have such a phenomenon at

all. Rather, it goes through a stable aging process and the efficiency gradually increases. This means that the SIG process is the only technology to make a device that reliably maintains the efficiency of a commercial－level device of 24% or more for more than 1000 hours, considering that the device is operated under the condition of being irradiated with light.
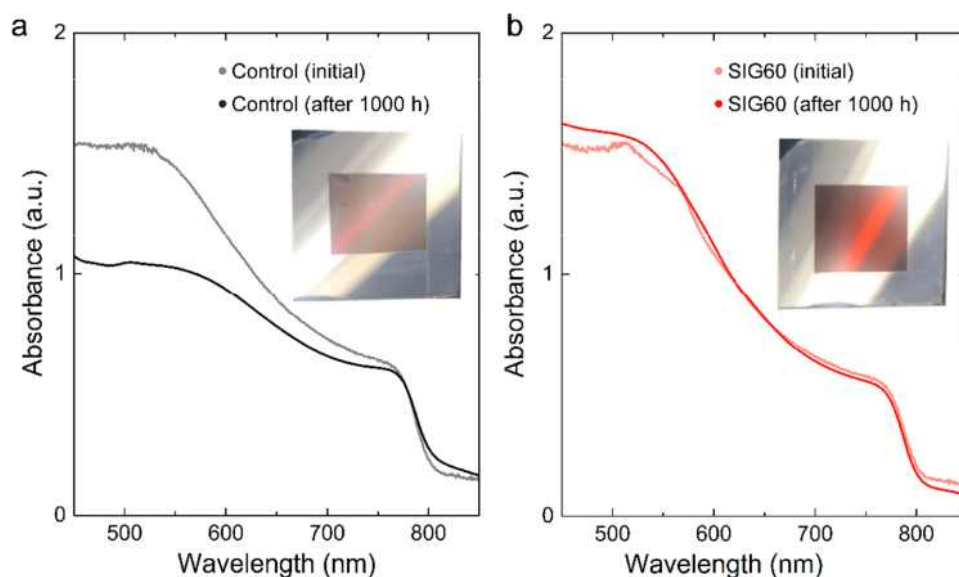
Figure 40. Stability tests were carried out with the control (a; FTO/SnO$_2$/3D) and SIG60(b; FTO/SnO$_2$/3D:SIG60−2D) films under 85% relative humidity at 25 ℃ in the dark. The pictures in panels are the control film and the SIG60 film after 1000h under the abovementioned condition, respectively. Fresh control and SIG60 films were measured just before exposure to 85% relative humidity at 25 ℃. After 1000 h of exposure under 85% relative humidity at 25 ℃ the films were removed from dark chamber to remeasure the UV−Vis absorption spectrum.
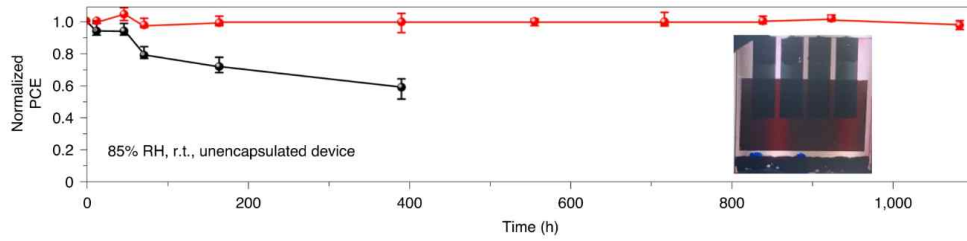
Figure 41. Efficiency degradation tracking of the unencapsulated control and SIG60 devices under 85% relative humidity (RH) at 25 ℃ in a dark chamber. The inset shows the condition of the device after 1,083 h. The initial average efficiency of the four cells are all over 20%.
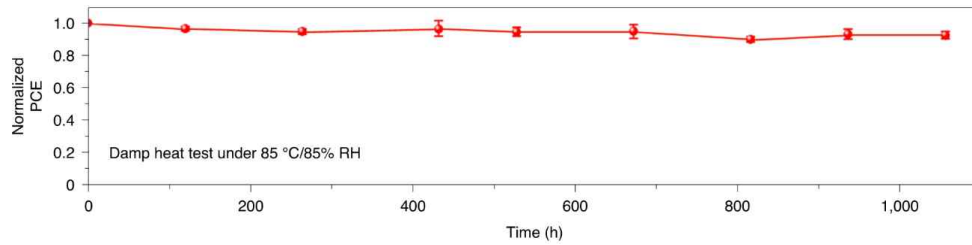

Figure 42. The results of the 1,056 h thermal stability test of the SIG60 device with encapsulation under 85% RH at 85 ℃ in the dark. The initial average efficiency of four cells are all over 21.70% The error bars in Figure 41 and 42 show the maximum and minimum bounds of normalized PCEs for four cells.
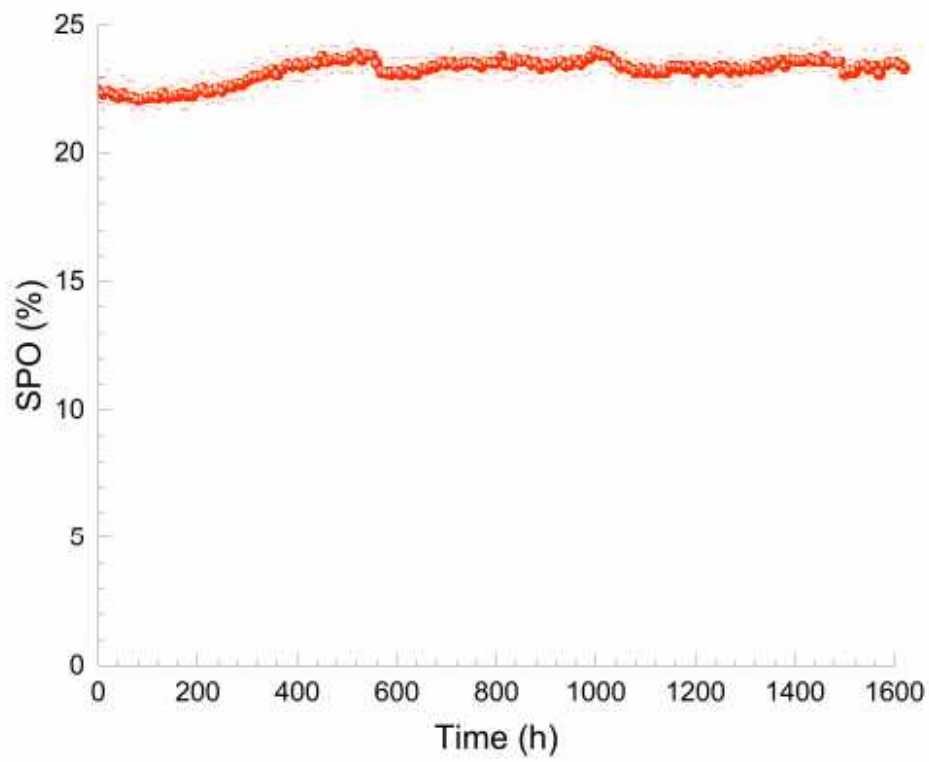
Figure 43. Stabilized power output (SPO) of SIG60 devices. Under simulated AM 1.5G (100 mW/cm2) encapsulated SIG60 devices was measured for 1620h at a fixed voltage in air. The fixed voltage was set to the maximum power point identified from the J−V curve (control: 0.98 V, SIG: 1.01 V). The error bars show the maximum and minimum efficiency for each measuring time.

4.3. Modulation

In order to succeed in a high-efficiency modulation device, of course, it is essential that all processes can be made into a large area. And it is necessary to have an appropriate laser compartmentalization technique to perform each process. In order to solve this process, the chemical bath depostion method of the SnO2-based electron transfer layer was easily solved. The deposition of electrodes and the application of 3D perovskite and hole transfer layers are also valid to some extent over a 7 square centimeter area (Figure 44). However, 2D perovskite is much lower packed than 3D perovskite, and its properties are much more organic, so it cannot achieve proper bonding with existing solvents. In fact, papers on donor number and dielectric constant have been published to point out this. Because the existing 2D itself does not fully understand its properties, large-area expansion has not been achieved, and the SIG process, a growth method, can be applied only after solving this problem. It is thought that the application will proceed easily because only appropriate pressure and reactants are required.
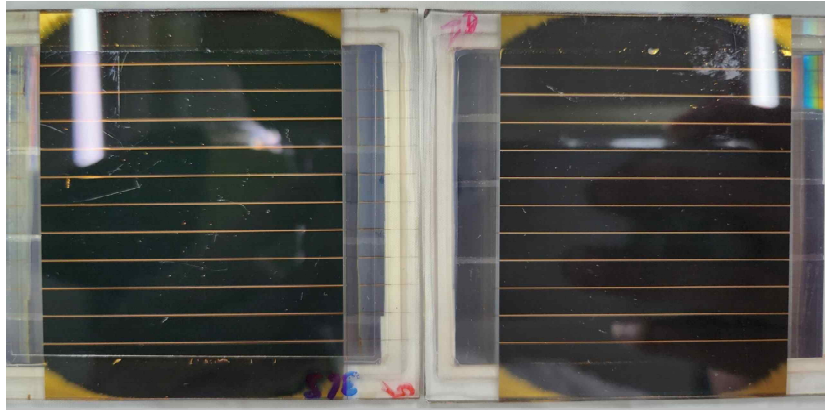
Figure 44. Image of 7x7 cm² metal halide perovskite solar cell module with encapculation

4.4. Conclusion

The stability issue has to do with how controllable perovskite can be, as it is a somewhat stable material by itself, but is very vulnerable to external factors. 2D perovskite exists in a much more stable state compared to its counterpart, so if you create a 2D:3D structure as a capping layer, you can secure stability very easily. The key technology is the SIG process, and a new paradigm has been proposed. Now, in order to succeed in commercialization, we have to succeed in large-area, the one remaining threshold that must be overcome. For this, it is important to understand the intrinsic properties of 2D perovskite to succeed in large-area development. If successful, it will become the most innovative and realistic technology for a large area.

4.5. References

[1] Schulz, P., Cahen, D., & Kahn, A. (2019). Halide perovskites: is it all about the interfaces?. Chemical reviews, 119(5), 3349−3417.

[2] Bailie, C. D., Unger, E. L., Zakeeruddin, S. M., Grätzel, M., & McGehee, M. D. (2014). Melt−infiltration of spiro−OMeTAD and thermal instability of solid−state dye−sensitized solar cells. Physical Chemistry Chemical Physics, 16(10), 4864−4870.

[3] Jena, A. K., Ikegami, M., & Miyasaka, T. (2017). Severe morphological deformation of spiro−OMeTAD in (CH3NH3) PbI3 solar cells at high temperature. ACS Energy Letters, 2(8), 1760−1761.

[4] Christians, J. A., Miranda Herrera, P. A., & Kamat, P. V. (2015). Transformation of the excited state and photovoltaic efficiency of CH3NH3PbI3 perovskite upon controlled exposure to humidified air. Journal of the American Chemical Society, 137(4), 1530−1538.

[5] Leguy, A. M., Hu, Y., Campoy−Quiles, M., Alonso, M. I., Weber, O. J., Azarhoosh, P., ... & Barnes, P. R. (2015). Reversible hydration of CH3NH3PbI3 in films, single crystals, and solar cells. Chemistry of Materials, 27(9), 3397−3407.

[6] Askar, A. M., Bernard, G. M., Wiltshire, B., Shankar, K., & Michaelis, V. K. (2017). Multinuclear magnetic resonance tracking of

hydro, thermal, and hydrothermal decomposition of CH3NH3PbI3. The Journal of Physical Chemistry C, 121(2), 1013-1024.

[7] Quintero-Bermudez, R., Gold-Parker, A., Proppe, A. H., Munir, R., Yang, Z., Kelley, S. O., ... & Sargent, E. H. (2018). Compositional and orientational control in metal halide perovskites of reduced dimensionality. Nature materials, 17(10), 900-907.

[8] Schlipf, J., Hu, Y., Pratap, S., Bießmann, L., Hohn, N., Porcar, L., ... & Mu̇ller-Buschbaum, P. (2019). Shedding light on the moisture stability of 3D/2D hybrid perovskite heterojunction thin films. ACS Applied Energy Materials, 2(2), 1011-1018.

Chapter 5. Conclusion

Solar cells are undeniably becoming a next-generation energy source. In it, perovskite is emerging as the No. 1 candidate, showing clear advantages. The final test will be how close to commercialization can be achieved while achieving efficiency and stability within an appropriate price. Thankfully, the dimensional approach called 2D perovskite shows a very good effect compared to the simple method. A device having a 2D:3D structure achieves stability and efficiency at the same time, and thanks to its stability, it is attracting attention as the most promising technology that can be adopted for commercialization. SIG technology, which has put an end to this approach, is currently receiving a lot of attention, but in fact has greater potential depending on how we nurture it. We have obtained a way to freely handle substances that are somewhere between inorganic and organic. This means that the application can be extended to all materials. If we can understand the various properties of 2D perovskite and analyze the SIG process on a scientific basis, this inevitably means occupation of the inorganic-organic interface. Currently, it has been shown that it can act as a technology that achieves superior efficiency for photovoltaic and

1 0 3

dramatically increases stability. In the future, it is hoped that heterojunction structures can be constructed and used more diversely through more applications and analysis.

Acknowledgments

초 록

   차세대 태양전지로 페로브스카이트 태양전지가 발돋움 하기 위해서는 효율과 안정성을 동시에 얻으면서 대면적화를 실현시켜줄 기술에 대한 연구가 필요하다. 이 때, 페로브스카이트의 유기 양이온을 조금 더 큰 스페이서로 바꾸는 것만으로도 할라이드 구조물은 파괴되지 않고 결정의 배열만 바꿔, 그 결과로 차원이 달라진 물질을 얻을 수 있는 점이 아주 흥미롭다. 이러한 방식으로 제작되는 이차원 페로브스카이트는 스페이서의 종류에 따라 그 다양성이 무궁무진함에도, 대부분의 이차원 페로브스카이트는 삼차원 페로브스카이트 보다 좀 더 유기화된 표면 상태를 가지고 있다. 이 특별한 표면은 외부 환경과 내부층을 차단하여 광활성층에 외부환경에 대한 저항성을 부여한다. 이러한 성질 때문에 이차원 페로브스카이트는 태양전지가 고질적으로 앓고 있던 안정성 문제를 해결하고자 했던 많은 연구자들의 관심을 받게 되었고, 해당 물질의 적절한 사용 방법에 대한 수많은 연구가 이루어 졌다. 그 과정에서 이차원 페로브스카이트 단독으로는 안정성과 효율의 상충효과가 있으나, 삼차원 페로브스카이트와 이차원 페로브스카이트 사이의 결합을 잘 조율하면 각 물질의 장점만을 얻을 수 있음이 발견된다. 그 구조를 이차원 페로브스카이트:삼차원 페로브스카이트 접합 구조라고 부르며, 해당 구조가 주는 추가적인 표면 결함제어효과로 페로브스카이트 단일 물질로 20 프로 이상의 상용화 수준의 효율을 가지는 태양전지가 제작되었다. 그러나, 이차원 페로브스카이트에 대한

미숙한 수준의 이해에 기반한 공정들을 통해서는 여전히 소자의 구동상태의 안정성까지 얻기엔 부족했다.

이에 필자는 고전적인 결정형성 이론에 근거한 고상전구체를 사용, 평면방향 성장방식(SIG 프로세스)을 고안하고, 이를 통해 온전한 이차원 페로브스카이트:삼차원 페로브스카이트 구조를 만드는데 성공한다. 해당 구조를 만드는 과정에서 계면손상을 제거할 뿐만 아니라 정공우세 물질이라는 특성을 이용하여 공핍층 최적화를 이루어 동일 물질을 통해 최적화된 소자 구조를 제시하였다. 해당 소자는 현재까지 이차원 페로브스카이트:삼차원 페로브스카이트 접합 구조를 이용한 태양전지 소자 중 가장 높은 효율을 국제 인증으로서 기록하고 있으며, 안정성 또한 세계 최고 수준을 보여주었다. 해당 기술은 이차원 페로브스카이트에 대한 성질을 이해하고, 성장원리를 수치화 하는 경우 단계적으로 추가로 발전 가능하며, 다양한 디바이스에 적용가능하다.

태양전지 소자는 현재 이미 샤클리−퀘이사 이론에 기반한 효율 이상의 구동성능을 보여주고 있다. 이는 소자 내부의발광 메커니즘에서 광재활용과 산란과 같은 빛을 여러 단계로 흡수하고 방출하기 때문이다. 이 사실을 인식한다면 우리는 태양전지를 좋은 발광체라는 관점에서 이해해야 하며, 이는 ELQE (Electroluminescence Quantum Efficiency)라는 전자가 얼마나 잘 빛으로 방출되는지 에 대한 값을 올리기 위해 더 노력해야 한다. 이를 위해 나는 샤클리−퀘이사 한계값을 넘어선 소자내에서 일어나는 광재활용과 산란에 대해 이해하고

이차원 페로브스카이트와 삼차원 페로브스카이트 내의 전하 확산도에 관한 측정법에 관해 연구하였다. SIG 프로세스 또한 두께 조절을 통해 소자내에서 분산손실되는 방출광의 양을 제어할 수 있는 방식이다. 또한 소자내로 입사되는 빛의 양을 늘릴 수 있는 빛 반사 방지막에 대한 연구도 수행하였다. 앞으로 2D 페로브스카이트의 합성이나 물성에 대한 연구를 지속하여 얻은 정보를 기반으로 이차원 페로브스카이트 : 삼차원 페로브스카이트 구조를 대면적 상용화 소자에 까지 이용가능한 수준으로 올리려는 시도를 계속할 것이다. 고안정성과 고효율을 유지하면서 상용화 가능한 소자를 구현하려면 페로브스카이트를 좋은 발광체로서 인식하고 소자 구조를 설계해야 하며, 이차원 페로브스카이트의 물성에 대한 연구가 필수적으로 선행되어야 한다.

주요어 : 이차원 페로브스카이트, 태양전지, 고효율, 고안정성, 고상공정
이차원:삼차원 구조
Student Number : 2017-28811

List of Publications

[1] **Jang, Y. W.**, Lee, S., Yeom, K. M., Jeong, K., Choi, K., Choi, M., & Noh, J. H. (2021). Intact 2D/3D halide junction perovskite solar cells via solid−phase in−plane growth. *Nature Energy*, 6(1), 63−71.

[2] Cho, C., **Jang, Y. W.**, Lee, S., Vaynzof, Y., Choi, M., Noh, J. H., & Leo, K. (2021). Effects of photon recycling and scattering in high−performance perovskite solar cells. *Science advances*, 7(52), eabj1363.

[3] Choi, J. S., **Jang, Y. W.**, Kim, U., Choi, M., & Kang, S. M. (2022). Optically and Mechanically Engineered Anti-Reflective Film for Highly Efficient Rigid and Flexible Perovskite Solar Cells. *Advanced Energy Materials*, 12(33), 2201520.

[4] Cho, C., Feldmann, S., Yeom, K. M., **Jang, Y. W.**, Kahmann, S., Huang, J. Y., ... & Greenham, N. C. (2022). Efficient vertical charge transport in polycrystalline halide perovskites revealed by four−dimensional tracking of charge carriers. *Nature Materials*, 1−8.

[5] **Jang, Y. W.**, Seo, G., & Choi, M. (2022). Solvent choice enables 2D: 3D bilayers toward stable perovskite solar cells. *Joule*, 6(11), 2454−2457.

[6] Park, M., Hong, S. C., **Jang, Y. W.**, Byeon, J., Jang, J., Han, M., ... & Lee, G. (2022). Scalable Production of High Performance Flexible Perovskite Solar Cells via Film−Growth−Megasonic−Spray−Coating System. *International Journal of Precision Engineering and Manufacturing−Green Technology*, 1−12.